OUKA
The University of Osaka
Institutional Knowledge Archive

Title	AMP-activated protein kinase-mediated gonadogenesis defect caused by Mg2+ dyshomeostasis
Author(s)	石井, 匡
Citation	大阪大学, 2017, 博士論文
Version Type	VoR
URL	https://doi.org/10.18910/61878
rights	
Note	

The University of Osaka Institutional Knowledge Archive : OUKA

https://ir.library.osaka-u.ac.jp/

The University of Osaka

AMP-activated protein kinase-mediated gonadogenesis defect caused by Mg^{2+} dyshomeostasis

Tasuku Ishii

March, 2017

Summary

AMP-activated protein kinase (AMPK) is an energy sensing kinase that regulates cellular metabolism to be adaptive to energy status. Here, I demonstrate the evolutionarily conserved functional interaction between AMPK and Mg^{2+} transporter cyclin M (CNNM). I isolated inactivating mutants for each of the five *Caenorhabditis elegans* (*C. elegans*) *cnnm* family genes, *cnnm-1* to *cnnm-5*. *cnnm-1; cnnm-3* double mutant worms demonstrated various phenotypes, among which the sterile phenotype was rescued by Mg^{2+} supplementation to the media. This sterility was caused by a gonadogenesis defect with severely attenuated proliferation of gonadal cells. Using this gonadogenesis defect as an indicator, I performed a non-biased genome-wide RNAi screening, to search for the genes associated with this phenotype. The results revealed that RNAi-mediated inactivation of several genes restores the elongation of gonads, including *aak-2*, which encodes the catalytic subunit of AMPK. I then generated triple mutant worms for *cnnm-1; cnnm-3; aak-2* and confirmed that the *aak-2* mutation also suppresses the defective gonadal development in *cnnm-1; cnnm-3* mutant worms. Thus, I provide genetic evidence linking Mg^{2+} homeostasis to energy metabolism via AMPK.

Table of contents

Abbreviations

AMPK	AMP-activated protein kinase
C. elegans	*Caenorhabditis elegans*
CBS	cystathionine–β–synthase
CNNM	cyclin M
DCT	distal convoluted tubule
DTCs	distal tip cells
DUF21	domain of unknown function 21
ICP-MS	inductively coupled plasma mass spectrometry
int.	intestinal
pc	pseudocoelom
PRL	phosphatase of regenerating liver
RNAi	RNA interference
TRP	transient receptor potential channel

General Introduction

Physiology of Mg^{2+} homeostasis

Mg^{2+} is the second most abundant cation in cells and serves as an essential cofactor for numerous enzymes. The average 70 kg person with 20% (w/w) fat has magnesium of about 24 g. Magnesium is widely distributed throughout the body, although bone contains high levels of magnesium: about 50–60% of total body magnesium is stored in the bone (Jahnen and Ketteler 2012). Cellular and organismal levels of magnesium are tightly regulated by the cooperative actions of various Mg^{2+} transporters and channels. Normally, the intracellular magnesium concentration is kept in the range of 5–20 mmol/L. The organismal magnesium level is generally assessed by measuring the serum magnesium concentration, which is normally in the range of 0.76–1.15 mmol/L (Jahnen and Ketteler 2012; Elin 2010). Perturbations of this homeostasis cause a wide variety of preclinical and clinical symptoms, including loss of appetite, lethargy, nausea, fatigue, vomiting, weakness, tremor, muscle spasms, tetany, and seizures (Jahnen and Ketteler 2012; Grober et al., 2015). It is also reported that chronic magnesium dyshomeostasis is associated with a number of diseases, including atherosclerosis, hypertension, cardiac arrhythmias, stroke, alterations in lipid metabolism, insulin resistance, type 2 diabetes mellitus, osteoporosis, depression, and other neuropsychiatric disorders (Castiglioni et al., 2013; Shah et al., 2014; Nielsen 2010; Chiuve et al., 2011; Larsson et al., 2012; Durlach 1990; Rosanoff and Plesset 2013; Curiel-Garcia et al., 2008).

Ancient conserved domain protein/Cyclin M (CNNM) family

CNNM family consists of 4 integral membrane proteins (CNNM1–4) in mammals. These proteins show a multi-domain structure, which is composed of a domain of unknown function 21 (DUF21) domain, a cystathionine–β–synthase (CBS) domain, a cyclic nucleotide monophosphate binding domain, and a sequence motif present in the cyclin box (Fig. 1A). Among these, the DUF21 domain and the CBS domain are evolutionally conserved from bacteria (Wang et al., 2003) (Fig. 1B). There have been many reports suggesting the functional relationship between CNNM and Mg^{2+} transport. *Salmonella* CNNM, CorC, has been suggested to participate in Mg^{2+} efflux (Gibson et al., 1991). The artificial expression of CNNM2 in *Xenopus* oocytes caused voltage-dependent transport of Mg^{2+} (Goytain et al., 2005). The expression of *Mefugu* CNNM3 in *Xenopus* oocytes decreased the cellular magnesium content (Islam et al., 2014). Moreover, recent studies showed that mammalian CNNM2 and CNNM4 can potently stimulate Mg^{2+} efflux when expressed in HEK293 cells and a weak level of Mg^{2+} efflux was also observed in cells expressing CNNM1 (Yamazaki et al., 2013; Hirata et al., 2014).

The *Cnnm* family genes are known to be responsible for the development of human hereditary diseases: mutations in *Cnnm2* cause familial dominant hypomagnesemia, a rare human disorder characterized by renal Mg^{2+} wasting (Stuiver et al., 2011) and mutations in *Cnnm4* cause Jalili syndrome, an autosomal recessive disease characterized by cone-rod dystrophy and amelogenesis imperfecta (Polok et al., 2009; Parry et al., 2009). In these diseases, several missense point mutations that change single amino acid residue in the CBS domain or the DUF21 domain are reported to occur. Therefore, these evolutionarily conserved domains are supposed to play important roles in the biological function of CNNM family. Indeed, *in vitro* experiments

indicated that amino acid substitutions of the corresponding residues abrogate the Mg^{2+} efflux function of CNNM proteins (Yamazaki et al., 2013; Hirata et al., 2014). Collectively, these results demonstrate that CNNM family is evolutionally conserved Mg^{2+} transporter family.

Caenorhabditis elegans (C. elegans)

In 1974, Sydney Brenner proposed *C. elegans* as a model organism to study primarily developmental biology and neurology (Brenner et al., 1974). Since then, it has been widely used in many laboratories because of its superior features as a model organism, as follows. *C. elegans* is a non-parasitic soil nematode. It can be easily propagated in the laboratory on agar plates or in liquid medium using *E. coli* as a food source. *C. elegans* mainly exists as hermaphrodites, which can self-fertilize, although males occasionally arise. As hermaphrodites can mate with males, the cross of different genotypes is possible. Moreover, *C. elegans* has a relatively short generation time of about 3.5 day at 20 ^{o}C (Fig. 2A), which facilitates crossing experiments compared to other model organisms, such as mice. Wild-type hermaphrodite adult worms contain a constant number of 959 somatic cells with invariant cell lineages and precise anatomical positions (Sulston and Horvitz 1977). Because they have a transparent and small body, the behavior of individual cells during development can be easily tracked using a microscope. In addition, both forward and reverse genetics are available in *C. elegans*, which enables to identify the gene(s) associated with some phenotypes at the organismal level. Particularly, the induction of RNA interference (RNAi) can be readily achieved by soaking the worms in dsRNA solution or by feeding the worms with bacteria expressing dsRNA (Tabara et al., 1998; Timmons and Fire 1998). Collectively,

these features allow me to use *C. elegans* as an ideal model for elucidating genes and pathways involved in various biological processes.

Gonadogenesis of *C. elegans*

Gonadogenesis of *C. elegans* has been widely studied for investigating various issues including morphogenesis, cell fate specification, cell cycle control, cell signaling, and programmed cell death (Hubbard and Greenstein 2000). A newly hatched *C. elegans* larva has a set of four cells, which are comprised of two germ cells (called as Z2 and Z3) flanked by two somatic gonadal cells (called as Z1 and Z4). The set of these four cells is called a primordium gonad and separated from the non-gonadal soma by a gonadal basal lamina (Kimble and Hirsh 1979; Sulston et al., 1983) (Fig. 2B, top). During the post embryonic development, Z1/Z4 divide and generate a total of 143 cells in hermaphrodite. The Z1/Z4 descendants form two U-shaped gonad arms, consist of two distal tip cells (DTCs) and two sheaths that house the germ line, two spermathecae, and a central uterus (Fig. 2B, bottom). DTCs, which are derived from Z1/Z4 distal daughter cells, are located at the distal end of two gonadal arms and lead the elongation of the arms to form U-shaped hermaphrodite gonad. In contrast, Z2/Z3 continue to divide throughout the larval development and give rise to the germ line.

Introduction

Mg^{2+} is the second most abundant cation in cells and serves as an essential cofactor for numerous enzymes. In mammals, magnesium levels are primarily regulated by intestinal absorption and renal reabsorption, where the epithelial cell layer permits selective and regulated Mg^{2+} transport between apical and basolateral surfaces. There are two known pathways for Mg^{2+} transport through the epithelial cell layers, the paracellular and the transcellular pathways (Schweigel and Martens, 2000). The transcellular pathway consists of apical entry and basolateral extrusion mediated by Mg^{2+}-permeable cation channels and transporters. TRPM6, a member of the transient receptor potential channel (TRP) family, is a key molecule in the transcellular pathway (Dimke et al., 2011). TRPM6 localizes at the apical membrane of intestinal epithelial cells and distal convoluted tubule (DCT) cells in the kidney (Voets et al., 2004), and mediates Mg^{2+} absorption and reabsorption, respectively. Indeed, mutations in *TRPM6* result in recessive familial hypomagnesemia with secondary hypocalcemia (Schlingmann et al., 2002; Walder et al., 2002). In addition, the related channel, TRPM7 was also found to play an important role in magnesium homeostasis in mice (Ryazanova et al., 2010). These observations implicate TRPM6/7 in the apical entry of Mg^{2+} into epithelial cells.

Another key molecule in the transcellular pathway is the ancient conserved domain protein/cyclin M (CNNM) family. In mammals, the CNNM family consists of 4 integral membrane proteins (CNNM1–4) that possess an evolutionarily conserved domain from bacteria (Wang et al., 2003). Recent genomic analyses have revealed that several single nucleotide polymorphisms in *CNNM*s are linked to serum magnesium

levels (Meyer et al., 2010) and that mutations in *CNNM2* are responsible for familial hypomagnesemia (Stuiver et al., 2011). It was reported that CNNM4 extrudes Mg^{2+} by stimulating Na^{+}/Mg^{2+} exchange and localizes to the basolateral membrane of intestinal epithelial cells (Yamazaki et al., 2013). Moreover, *CNNM4*-deficient mice displayed defective intestinal Mg^{2+} absorption. These observations suggest that CNNM4 mediates transcellular Mg^{2+} transport by basolateral Mg^{2+} extrusion in the intestinal epithelia. Another family member, CNNM2, is strongly expressed at the basolateral membrane of DCT cells (Stuiver et al., 2011; de Baaij et al., 2012) and can also extrude Mg^{2+} like CNNM4 (Hirata et al., 2014), suggesting that CNNM2 plays a similar role in basolateral Mg^{2+} extrusion in kidney DCT cells.

Two groups recently reported that CNNMs associate with phosphatase of regenerating liver (PRL), a cancer-associated tyrosine phosphatase (Funato et al., 2014; Hardy et al., 2015). However, how PRL affects the function of CNNMs remains controversial. In addition, it is unknown whether other molecules are also involved in the regulation of CNNM function. Artificial overexpression of PRL in cultured cells stimulates various signaling pathways involved in the regulation of cell proliferation (Al-Aidaroos and Zeng, 2010; Rios et al., 2013), suggesting that the abnormality of Mg^{2+} regulation by CNNMs can influence the signaling pathways. However, little is known regarding its mechanism of action. To address these problems, non-biased comprehensive screening for genes that functionally associate with CNNMs is expected to serve as a powerful strategy. *Caenorhabditis elegans* (*C. elegans*), which has been used as a model organism for genetic analyses, also absorbs Mg^{2+} by a similar transcellular mechanism in the intestine. The apical entry step of the transcellular pathway is mediated by two TRPM family channels GTL-1 and GON-2 (Teramoto et al.,

2005). *C. elegans* also has an excretory canal analogous to the mammalian kidney, which removes wastes from the body, wherein another *C. elegans* TRPM channel GTL-2 plays an important role in magnesium homeostasis (Teramoto et al., 2010). Thus, *C. elegans* possesses a system for regulating magnesium homeostasis similar to mammals. Taken together with the genetic tractability of *C. elegans*, this organism should serve as an ideal experimental model to investigate the regulatory mechanism and functional importance of magnesium homeostasis.

In this study, I performed functional analyses of the *C. elegans* CNNM family and found that *cnnm-1; cnnm-3* double mutant worms displayed pleiotropic phenotypes. Of these, the sterile phenotype (due to defective gonadogenesis) was restored by Mg^{2+} supplementation. Detailed analyses of the gonadal phenotype revealed that the inactivating mutation of *aak-2*, which encodes the α subunit of AMP-activated protein kinase (AMPK), significantly rescued the gonadogenesis defect in *cnnm-1; cnnm-3* mutants, thereby indicating genetic interaction between CNNM and AMPK.

Results

cnnm family genes of *C. elegans*

A homology search using BLAST with amino acid sequences of the human CNNM family proteins revealed that the *C. elegans* genome contains genes encoding 5 previously uncharacterized CNNM family proteins, which possess the functionally essential domains, DUF21 and CBS (Yamazaki et al., 2013; Hirata et al., 2014) (Fig. 3). Each *C. elegans* CNNM protein showed significant identity with all human CNNM family members (24–47%). To investigate the *in vivo* functions of *C. elegans* CNNM family proteins, I obtained and generated mutant alleles for all *cnnm* family members (Fig. 3). *cnnm-1(gk222902)* contains a point mutation that introduces a premature stop codon in the DUF21 domain. *cnnm-2(dcr1)*, *cnnm-3(dcr2)*, and *cnnm-4(dcr3)* alleles show deletion of 162, 289, and 173 nucleotides, respectively, in either the DUF21 or the CBS domain. In the *cnnm-5(ttTi19567)* allele, the *Mos 1* sequence is inserted in the second exon of *cnnm-5*, resulting in a truncated product that lacks both the DUF21 and CBS domains. Therefore, these mutations are considered to abolish the function of each CNNM protein.

Pleiotropic phenotypes of *cnnm-1; cnnm-3* mutant worms

I then observed these mutant worms and found that they all showed no obvious abnormalities except for the *cnnm-3* mutant worms, a few (5.3%) of which were sterile (Fig. 4A). I speculated that functional redundancy among the *cnnm* family members might mask the mutant phenotype. Thus, I generated double mutants for all possible combinations by crossing every single mutant. I found that *cnnm-1; cnnm-3* and

cnnm-2; cnnm-3 mutant worms were respectively severely (100%) and moderately (22%) sterile (Fig. 4A). Because of the completely sterile phenotype, I focused on the analyses of *cnnm-1; cnnm-3* mutants in the following experiments.

I noticed that the *cnnm-1; cnnm-3* mutant worms were significantly smaller than the wild-type N2 worms grown for the same time (Fig. 4B). Therefore, I attempted to compare the body size of stage-matched worms. *cnnm-1; cnnm-3* mutant worms did not form the vulva (Fig. 4B, right), the eversion of which determines the adult stage (Sharma-Kishore et al., 1999). Therefore, I focused on the presence of alae, the longitudinal ridges present in adult worms but not in earlier L2−4 larvae (Fig. 4C), as the marker to confirm whether the worms reached the adult stage (Sulston and Horvitz, 1977; Singh and Sulston, 1978). I examined alae formation and body size of mixed stage worms from L2 to adult, and then estimated the body size at the transition from L4 to adult molt, which was determined as the mean value of body size of the three smallest worms with alae and the three largest worms without alae. The results showed that the body size of *cnnm-1; cnnm-3* mutant worms was smaller than that of wild-type worms (Fig. 4D). At 64 hours when all wild-type worms had just reached the adult stage, 58.5% of the *cnnm-1; cnnm-3* mutant worms were alae-positive, indicating the occurrence of developmental delay (Fig. 4E).

I also noticed that the color of the intestine in *cnnm-1; cnnm-3* mutant worms was dark (Fig. 4B, right). This phenomenon was also observed in mutant worms of *daf-2*, encoding the insulin-like receptor (Kenyon et al., 1993). Since *daf-2* mutations are famous for causing elevated fat storage and lifespan extension (Kimura *et al.* 1997; Kenyon *et al.* 1993), I first examined fat storage of *cnnm-1; cnnm-3* mutant worms (Fig. 5). Staining of fixed worms with Nile Red, a lipophilic fluorescent dye, is one of

established methods for assessing fat levels of worms (Brooks et al., 2009). As previous studies, *daf-2* mutant worms showed higher levels of fat storage than wild-type worms, whereas *cnnm-1; cnnm-3* mutant worms had much higher levels of fat than *daf-2* mutants. I next examined the lifespan of *cnnm-1; cnnm-3* mutant worms (Fig. 6). Consistent with previous studies, *daf-2* mutant worms showed much longer lifespan than wild-type worms. In contrast, *cnnm-1; cnnm-3* mutant worms had shorter lifespan than the wild-type worms, which was comparable to that of the short-lived mutants of *daf-16*, which encodes a FOXO-family transcription factor (Kenyon et al., 1993). All these phenotypes of *cnnm-1; cnnm-3* mutant worms were rescued by the introduction of either *cnnm-1* or *cnnm-3* genomic DNA (Figs. 4A, 4D, 5, and 6), confirming that these abnormalities are caused by mutations in *cnnm-1* and *cnnm-3*.

Effects of Mg^{2+} supplementation on *cnnm-1; cnnm-3* mutant worms

Since mammalian CNNM family proteins are involved in Mg^{2+} transport (Yamazaki et al., 2013; Funato et al., 2014; Hirata et al., 2014), the phenotypes of *cnnm-1; cnnm-3* mutant worms could possibly be due to some abnormality in magnesium homeostasis. Therefore, I tested the effects of Mg^{2+} supplementation in the media, and found that 76.6% and 100% of *cnnm-1; cnnm-3* mutant worms became fertile by supplementation with 1 mM and 3 mM of Mg^{2+}, respectively (Fig. 7A). I also found that supplementation of 1 mM Mg^{2+} significantly suppressed increased fat storage in *cnnm-1; cnnm-3* mutant worms (Fig. 7B). In contrast, the small body size and the short lifespan were not affected by Mg^{2+} supplementation (Figs. 7C and 7D). Supplementation of culture plates with Ca^{2+} did not affect any of the phenotypes. Collectively, these results suggest that the sterile and increased fat storage phenotypes

of *cnnm-1; cnnm-3* mutant worms are related to altered magnesium homeostasis.

Dysregulation of DAF-16 or alteration of food intake are not responsible for the increased fat storage caused by *cnnm-1; cnnm-3* mutation

To further characterize the role of CNNM-1 and CNNM-3 in fat metabolism, I first investigated whether the amount of food consumption of *cnnm-1; cnnm-3* mutant worms increased (Fig. 8A). The pharyngeal pumping rate of *cnnm-1; cnnm-3* mutant worms was normal, suggesting that the increased fat storage in *cnnm-1; cnnm-3* mutant worms is not due to the result of an alteration in food intake. The increased fat storage in *daf-2* mutant worms is abolished by mutations in the downstream gene *daf-16*, encoding the FOXO transcription factor (Ogg et al., 1997). Therefore, I next generated triple mutant worms for *cnnm-1; cnnm-3; daf-16*, and examined fat storage by Nile Red staining (Fig. 8B). I found that the additional mutation in *daf-16* had no effect on fat storage in *cnnm-1; cnnm-3* mutant worms, suggesting that the fat accumulation is not due to an altered insulin-like signaling pathway. Since it is generally known that reduced or abolished reproduction can lead to increased fat storage in *C. elegans* (O'Rourke *et al.* 2009), there is a possibility that the increased fat storage phenotype occurs secondary to the fertility defect. Therefore, I next focused on the sterile phenotype for further analyses. As the *cnnm-1; cnnm-3* mutant worms had neither oocytes nor vulva (Fig. 4B), which are formed during gonadal development, I next examined gonadal development in *cnnm-1; cnnm-3* mutant worms.

***cnnm-1* and *cnnm-3* are required for postembryonic gonadal development**

At hatching, the primordial gonad in *C. elegans* is composed of four cells, namely Z1–

Z4 cells (Kimble and Hirsh, 1979). During the larval development, Z1 and Z4 cells give rise to the somatic gonad including the DTCs, uterus, sheath cells, and spermathecae, whereas the Z2 and Z3 cells give rise to the germ line. I examined the extent of gonadal development by expressing GFP under the control of the *lag-2* promoter, which drives gene expression in Z1/Z4 cells and in DTCs (Mathies et al., 2004; Blelloch et al., 1999) that are located at the distal end of two gonadal arms and lead the elongation of the arms to form U-shaped hermaphrodite gonad. When the mutant worms hatched from eggs, two GFP-positive cells that correspond to Z1/Z4 cells were observed at the appropriate positions, suggesting that the development of the primordial gonad proceeds normally in mutants. However, the primordial gonad of mutants did not elongate even at the L4/young adult stages (Fig. 9A). Immunofluorescence analysis using an anti-PGL-1 antibody, which stains P-granules in germ cells demonstrated that the majority of *cnnm-1; cnnm-3* mutant L4/young adult worms had only two germ cells that correspond to the Z2/Z3 cells (Fig. 9B). Considering that Mg^{2+} supplementation restored the fertility of *cnnm-1; cnnm-3* mutant worms, these results suggest that CNNM-1 and CNNM-3 promote postembryonic gonadal development through regulation of Mg^{2+} levels. Previous studies have demonstrated that mutants of *gon-2*, which encodes a TRPM channel protein, showed a severe gonadogenesis defect, which was partially restored by Mg^{2+} supplementation (Sun and Lambie, 1997; Teramoto et al., 2010).

Localization of CNNM-1 at the basolateral membrane of intestinal cells

To characterize the role of CNNM-1 and CNNM-3, I first examined their expression pattern by generating transgenic worms expressing GFP under the control of the *cnnm-1* or *cnnm-3* promoters. Unique GFP expression was observed in various tissues, such as

the pharynx, hypodermis, rectum, and muscles, but strong expression was commonly observed in the intestine and the neurons (Fig. 10A). Given this expression pattern, I forced the expression of CNNM-1 in the intestine or the neurons of *cnnm-1; cnnm-3* mutant worms, using the intestine-specific *ges-1* promoter (Edgar and McGhee, 1986) or the neuron-specific *aex-3* promoter (Iwasaki et al., 1997), respectively. The intestinal expression of CNNM-1 almost completely rescued the sterile phenotype of *cnnm-1; cnnm-3* mutants, whereas its expression in the neurons was ineffective (Fig. 10B), suggesting that CNNM-1 expression in the intestine is important for gonadal development. The intestinal cells of *C. elegans* are attached to each other at the borders of the apical membrane by cell-cell junctions called apical junctions, which have mixed traits of both the adherens junction and the tight junction in mammalian epithelial cells, and thus have apico-basal polarity (Cox and Hardin, 2004). I subsequently examined the subcellular localization of CNNM-1 in intestinal cells using transgenic worms expressing Venus-fusion proteins of CNNM-1, which also rescued the sterile phenotype (Fig. 4A). Excluding some large clumps in the cytoplasm, which are often observed upon ectopic expression of Venus-fusion proteins, the fluorescent signal was predominantly observed in the basolateral membrane of intestinal cells (Fig. 10C). Therefore, CNNM-1 is considered to mediate Mg^{2+} absorption from the intestinal lumen by extruding Mg^{2+} from intestinal cells to the pseudocoelom (Fig. 10D). Based on this hypothesis, *cnnm-1; cnnm-3* mutant worms should have higher levels of Mg^{2+} in intestinal cells and lower levels of Mg^{2+} in the pseudocoelom that contains other tissues such as the gonad, which may explain why Mg^{2+} supplementation restored gonadal development (Fig. 7A).

Assessment of magnesium levels by ICP-MS

To assess the predicted regulatory model of Mg^{2+} levels, I quantified the magnesium levels in wild-type worms and in *cnnm-1; cnnm-3* mutant worms using inductively coupled plasma mass spectrometry (ICP-MS). As shown in Table 1, I found that *cnnm-1; cnnm-3* mutant worms had higher magnesium levels (143% of wild-type worms). I then physically dissected the intestines from the worms using a scalpel and subjected them to magnesium quantitation. The results indicated much higher levels of magnesium in *cnnm-1; cnnm-3* mutant worms (195% of wild-type worms). It was technically difficult to physically dissect other remaining tissues, which are much smaller than the intestine. Therefore, I estimated magnesium levels in other tissues by calculating the volumes of the total body and the intestine, and found that the magnesium level was significantly reduced in other tissues of *cnnm-1; cnnm-3* mutant worms (67% of wild-type worms). Collectively, these results are consistent with the predicted model indicating increased magnesium in the intestine and decreased magnesium in other tissues (Fig. 10D).

RNAi screening for genes that functionally associate with *cnnm-1* and *cnnm-3*

Next, I performed genome-wide screening using an RNAi feeding library targeting 86% of the open reading frame of *C. elegans*, to search for genes that functionally associate with *cnnm-1* and *cnnm-3*. To increase RNAi efficacy, screening was performed using worms that also carry the *rrf-3* mutation, which renders the worms hypersensitive to RNAi treatment (Simmer et al., 2003). Two rounds of screening identified 31 genes, of which RNAi treatment reproducibly resulted in elongation of gonadal arm in more than 50% of *cnnm-1* ; *cnnm-3* ; *rrf-3* mutant worms (Table 2 and Fig. 11). These 31 genes are

involved in a variety of biological processes, including protein transport, metabolism, mitochondrial function, signal transduction, gene expression, ion transport, immune response, and the cell cycle. Among these, I chose to perform detailed analyses on *aak-2*, encoding α-subunit of AMPK. AMPK is the key energy sensor in most eukaryotic cells, and is activated under low-energy conditions such as decreased ATP levels (Hardie et al., 2012). The majority of the intracellular ATP is known to form complexes with Mg^{2+}, which is required for numerous enzymatic reactions that use ATP (Romani, 2011; Günther, 2006). These observations led me to consider that dysregulation of cellular Mg^{2+} levels in *cnnm-1; cnnm-3* mutant worms could affect AMPK activity.

AMPK mediates the gonadogenesis defect caused by *cnnm-1; cnnm-3* mutation

AMPK is a heterotrimeric kinase, consisting of a catalytic subunit (α) and two regulatory subunits (β and γ). In *C. elegans*, there are two α subunits, AAK-1 and AAK-2, which are encoded by different genes (Apfeld et al., 2004). Therefore, I examined whether the predicted null mutations for *aak-1* and/or *aak-2* could suppress the gonadogenesis defect in *cnnm-1; cnnm-3* mutant worms (Fig. 12A). The additional mutation in *aak-2* or in both *aak-1* and *aak-2* almost totally suppressed the gonadogenesis defect, while *aak-1* mutation showed only a marginal effect. Moreover, I analyzed germ cell proliferation in *cnnm-1; cnnm-3; aak-1; aak-2* quadruple mutant worms and found that most of them contained many germ cells (> 100 cells, Fig. 12B). These results indicate that the gonadogenesis defect caused by Mg^{2+} deficiency was mediated by AMPK containing each of the two α subunits, but predominantly the α2 subunit encoded by *aak-2*. Overall, this study clarified the evolutionarily conserved regulation of AMPK by the CNNM family from nematodes to mammals.

Discussion

In this study, I have shown that *cnnm-1; cnnm-3* mutant worms displayed pleiotropic phenotypes, such as infertility due to a gonadogenesis defect, increased fat storage, shortened life span, and small body size (Figs. 4–6). Among these, the gonadogenesis defect and increased fat storage phenotypes were almost completely restored by Mg^{2+} supplementation to the culture media (Fig. 7). These results suggested that abnormal Mg^{2+} regulation in *cnnm-1; cnnm-3* mutant worms affects gonadal development and the fat metabolism. It is generally considered that the increased fat storage can occur as the result of impaired reproduction (Hansen *et al.* 2013). The loss of germline proliferation by a mutation of *glp-1*, encoding a member of the LIN-12/Notch family of receptors, induces extensive fat accumulation (O'Rourke *et al.* 2009). Therefore, the increased fat storage phenotype of *cnnm-1; cnnm-3* mutant worms may occur secondary to the fertility defect, which led me to focus on the gonadal development. It is also known that infertility is intimately associated with longevity in *C. elegans* (Hansen et al., 2013). Indeed, germline-less worms generated by *glp-1* mutations or laser ablation exhibit significantly prolonged lifespan (Arantes-Oliveira et al., 2002; Hsin and Kenyon, 1999). In contrast, infertile *cnnm-1; cnnm-3* mutant worms had a shorter lifespan than wild-type worms. In addition, Mg^{2+} supplementation did not affect the lifespan of *cnnm-1; cnnm-3* mutants, even though the worms became fertile (Fig. 7). Therefore, the reduced lifespan phenotype in *cnnm-1; cnnm-3* mutants occurs independently of abnormal fertility. The small body size phenotype of *cnnm-1; cnnm-3* mutants was also not affected by Mg^{2+} supplementation (Fig. 7). At present, whether the life span and body size phenotypes are related to altered Mg^{2+} homeostasis is unknown, and further

analyses are required to clarify the relationship with CNNM functions.

My elemental analyses suggested that the *cnnm-1; cnnm-3* mutant worms had higher levels of Mg^{2+} in intestinal cells and lower levels of Mg^{2+} in the pseudocoelom that contains other tissues such as the gonad (Table 1). This is consistent with the presumed molecular function of CNNM proteins at the basolateral membrane of intestinal epithelia (Fig. 10). In addition, I found that *cnnm-1; cnnm-3* mutants exhibited a severe proliferation defect in gonadal cells (Fig. 9), which was completely restored by additional Mg^{2+} supplementation to the media. Collectively, these results strongly suggest that the proliferation defect of gonadal cells is due to Mg^{2+} deficiency in the gonad. The importance of Mg^{2+} in regulation of cell proliferation has long been proposed (Rubin, 1975; Rubin, 2007). A study on cells lacking TRPM7, a Mg^{2+}-permeable cation channel, revealed the significance of Mg^{2+} influx for maintaining cell proliferation (Sahni and Scharenberg, 2008). However, how Mg^{2+} affects cell proliferation is poorly understood. A previous study showed that higher intracellular Mg^{2+} levels can lead to increased intracellular ATP levels and decreased AMPK activity in cultured mammalian cells (Funato et al., 2014), suggesting the molecular linkage of Mg^{2+} to AMPK. I here performed a non-biased genome-wide RNAi screen to identify the genes involved in Mg^{2+}-associated regulation of cell proliferation, which yielded 31 candidate genes including *aak-2*, which encodes a catalytic subunit of AMPK (Table 2). Moreover, I confirmed the importance of *aak-2* by showing that *aak-2* mutation restored the proliferation of gonadal cells in *cnnm-1; cnnm-3* mutants (Fig. 12). Therefore, I provided solid genetic evidence linking Mg^{2+} homeostasis to the AMPK function in the regulation of cell proliferation, which is evolutionarily conserved from nematodes to humans.

Besides *aak-2*, my RNAi screen yielded several candidate genes, which are involved in various biological processes. These candidate genes included *aps-2* and *dpy-23*, which encode the essential subunits of the core component of clathrin-mediated endocytosis, AP2 adaptor complex (Traub, 2009). Among the 31 candidate genes, 4 genes (*aps-2*, *dpy-23*, *did-2*, and *wwp-1*) were assigned to have the Gene Ontology term of "endocytosis" in DAVID Bioinformatics Resources (http://david.abcc.ncifcrf.gov/). In addition, 5 other genes (*hpo-5*, *hpo-19*, *dbr-1*, F29A7.6, and F58B3.4) are also supposed to participate in endocytosis because their RNAi-inactivation disrupted endocytosis in *C. elegans* (Balklava et al., 2007). One major cellular role of endocytosis is to attenuate the signaling activity of cell surface receptors (Polo and Di Fiore, 2006; Sorkin and von Zastrow, 2009). Taken together with the findings of this study, Mg^{2+} homeostasis may also affect the endocytic machinery. Further characterizations of the relationship between Mg^{2+} and these endocytosis-related genes may reveal this intriguing mechanism.

Methods

C. elegans strains and general methods for handling worms

All *C. elegans* strains used in this study were derived from wild-type *C. elegans* var. Bristol (N2). Unless otherwise indicated, worms were grown at 20°C on NGM-lite plates seeded with OP-50 *E. coli*, as described previously (Sun and Lambie, 1997). The following mutations, rearrangement, and transgenes were used in this study: LGI *cnnm-4(dcr3)* and *daf-16(mgDf50)*; LGII *rrf-3(pk1426)*; LGIII *daf-2(e1370)*, *cnnm-5(ttTi19567)*, and *aak-1(tm1944)*; LGIV *cnnm-1(gk222902)* and *nT1[qIs51]* (IV; V); LGX *cnnm-3(dcr2)*, *cnnm-2(dcr1)*, and *aak-2(ok524)*; *qIs56[lag-2p::GFP]*; *sEx14584[rCesC33D12.2::GFP]*. Strains carrying each mutation and rearrangement were backcrossed at let 4 times with N2 before use. Double homozygous worms for *cnnm-1(gk222902)* and *cnnm-3(dcr2)* are completely sterile, and therefore, *cnnm-1(gk222902)/+; cnnm-3(dcr2)* worms were maintained using the *nT1[qIs51]* (IV; V) balancer. Synchronization of worm development was achieved by egg laying of gravid adults for 6 h, unless otherwise indicated.

Generation of plasmids and transgenic *C. elegans* lines

To generate *cnnm-1p::GFP*, the 4,333 bp fragment of the 5′ region of *cnnm-1* was amplified by PCR and then inserted into the GFP expression vector pPD95.77 (kindly provided by A. Fire). To generate the *cnnm-1* genomic construct, the *cnnm-1* genomic fragment (−4,933 to +7,492 relative to the ATG start codon) was obtained by restriction enzyme digestion from the fosmid WRM0636cE07 (Dnaform). The remaining portion of the *cnnm-1* genomic fragment (+7,493 to +8,924) was generated by PCR

amplification. As for the *cnnm-3* genomic construct, the *cnnm-3* genomic fragment (−2,935 to +4,090) was obtained by PCR amplification. Thereafter, each genomic fragment was inserted into pBluescript KS (stratagene). For the *cnnm-1*::*Venus* translational fusion construct, the same fosmid fragment as that used for the *cnnm-1* genomic construct was linked to the *cnnm-1* genomic fragment (+7,493 to +8,610) generated by PCR amplification. The fragments were then inserted into pPD95.79-Venus (kindly provided by T. Ishihara). For the expression of *cnnm-1* under the control of the *ges-1* promoter or the *aex-3* promoter, *cnnm-1* cDNA was prepared by RT-PCR and then inserted into pDEST-*ges-1p* and pDEST-*aex-3p,* kindly provided by H. Kuroyanagi (Kuroyanagi et al., 2006, 2010). The DNA sequences of all PCR products were confirmed by sequencing. To generate transgenic lines, plasmids were injected into N2 or *cnnm-1(gk222902)/nT1[qIs51]; cnnm-3(dcr2)* along with *rol-6(su1006)* (Mello et al., 1991) or *rab-3p::mCherry* (Addgene) as an injection marker.

Isolation of *cnnm* mutant strains

The mutant strains of *cnnm-2(dcr1)*, *cnnm-3(dcr2)*, and *cnnm-4(dcr3)* in this study were isolated from the Trimethylpsoralen/UV-mutagenized library by performing nested PCR as described previously (Kubota et al., 2004). The primer sets used for screening were as follows: *cnnm-2* first round; 5′-TGTCCCGTTTGATGGAAAAT-3′ and 5′-TTTGGAACTATCGTGCCTCC-3′; *cnnm-2* second round; 5′-CGAGGATGGTAGAAATGCTCA-3′ and 5′-TACCTGTGGCATCATGGTTG-3′. *cnnm-3* first round; 5′-TTGATTAGCGGCAATAAGGG-3′ and 5′-ATATGCCAAAATGGCTTTCG-3′; *cnnm-3* second round; 5′-GCTCACCATTCAACGATTCA-3′ and 5′-ATGAACTCACGAGGTGTCGG-3′.

cnnm-4 first round; 5′-CATTTTTCAGCGAGCCTTTC-3′ and 5′-CCCATCTTCTTCCGAATCAA-3′; *cnnm-4* second round; 5′-CTTTGCCTCGGTTTATCTGC-3′ and 5′-AGACGTGAATGGCCTTGTTC-3′. The *cnnm-1(gk222902)* and the *cnnm-5(ttTi19567)* alleles were generated by the *C. elegans* Reverse Genetics Core Facility at the University of British Columbia and the NEMAGENETAG Project funded by the European Community (Vallin et al., 2012), respectively.

Germ cell counts

Germ cells were stained as previously described (Kawasaki et al., 1998) with slight modifications. L4/young adults were permeabilized using the freeze–crack method and sequentially fixed in cold methanol for 10 min and in cold acetone for 10 min. The samples were blocked with 2% bovine serum albumin in PBS-T (PBS containing 0.05% Tween 20) for 30 min at room temperature, and then incubated overnight at 4^{o}C with mouse anti-PGL-1 antibody K76 (1:20 dilution), developed by S. Strome (Strome and Wood, 1983) and provided by the Developmental Studies Hybridoma Bank. This was followed by incubation with Alexa Fluor 568 goat anti-mouse IgG (1:2000 dilution, Invitrogen) for 2 h at room temperature. Coverslips were mounted on a microscopic glass slide. Thereafter, the samples were observed using a microscope, and PGL-1 positive cells were counted as germ cells.

Gonadal arm extension

To analyze the gonadal arm extension, *lag-2p::GFP* was used to visualize the Z1/Z4 cells and DTCs. The worms were analyzed at the L4/young adult stage using a

microscope. I defined worms with gonads of ≧ 60 μm in length of the long axis (3-fold length of the primordial gonad) as extended.

Nile Red staining

Nile Red staining was performed as described previously (Yen et al, 2010) with slight modifications. Day 3 adult worms were washed twice with PBS and then suspended in 120 μl of PBS and 120 μl of 2 × MRWB buffer (160 mM KCl, 40 mM NaCl, 14 mM Na_2EGTA, 30 mM PIPES (pH 7.4), 1 mM spermidine, 0.4 mM spermine, 2% paraformaldehyde, 0.2% 2-mercaptoethanol). The worms were subjected to 3 freeze-thaw cycles by using liquid nitrogen and a water bath at 37°C, followed by washing with PBS to remove paraformaldehyde. The worms were stained overnight at room temperature in Nile Red solution diluted in water (0.1 μg/ml final concentration, Invitrogen) and then washed twice with PBS, followed by mounting on a 3% agarose pad on a microscopic glass slide for microscopic observation and photography. All fluorescent images were obtained with identical illumination and exposure parameters. The quantification of Nile Red staining was performed using Image J (NIH software). Original images were converted to binary ones to separate the worm section from the background. Subsequently, the worm section was automatically outlined and then, the mean fluorescence intensity per area was calculated from the original images, followed by subtraction of mean background signal.

Measurement of pharyngeal pumping rates

Pharyngeal pumping rates were measured as previously described (Srinivasan et al., 2008), with slight modifications. L4/young adult worms were examined. Their

pharyngeal contractions during 10 sec were manually counted by observing with a microscope, and then pharyngeal pumping rates per minute were calculated.

Lifespan assay

Lifespan assay was performed as described previously (Kenyon et al., 1993) with slight modifications, starting with L4/young adults. To remove the contamination of progeny, worms were transferred to fresh NGM-lite plates seeded with OP-50 every 2 days until day 8, after which only those worms on plates where progeny was observed were transferred. Survival was monitored daily. Worms that did not move, respond to nose touch with a platinum picker, or exhibit pumping were determined as dead and were removed. Worms that crawled off the plate, had a protruded vulva, or died by internal hatching were excluded.

Body size measurement

Mixed stage worms from L2 to adult (L4 to adult worms comprise the most) were anesthetized with M9 buffer containing 50 mM NaN_3 and were mounted on a 3% agarose pad on a microscopic glass slide. Thereafter, the worms were examined for alae formation using a microscope and then photographed for body size measurement. The area of the worms was directly measured from the images using Image J (NIH software). The body size at the transition from L4 to adult molt was determined by calculating the mean body size of the smallest three worms with alae and the largest three worms without alae.

Genome wide RNAi screening

Feeding RNAi was performed as described previously (Kamath et al., 2001). In total, 15,357 bacterial RNAi feeding strains from the Ahringer library (Kamath et al., 2003) were tested as follows in the first round screening (n = 5–10 worms per strain), using bacteria carrying empty vector L4440 (kindly provided by A. Fire) as the negative control. *cnnm-1(gk222902)/nT1[qIs51]; cnnm-3(dcr2); rrf-3(pk1426); qIs56[lag-2p::GFP]* gravid adults were bleached, and synchronized P0 worms at the L1 stage were transferred to RNAi plates. The F1 progeny lacking the balancer *nT1[qIs51]* (without pharyngeal GFP expression) were phenotypically scored at the L4/young adult stage as described in the "Gonadal arm extension" section. RNAi clones were scored as positive if gonadal arms extended in more than 50% of the worms in the F1 generation. Some clones resulted in larval arrest or in sterile phenotypes in the P0 generation, and therefore, these clones were scored in the P0 generation. The first round screening led to the identification of 119 positive clones, which were re-tested as described above in the second round screening (n = 30 worms per strain).

ICP-MS

For measurement of magnesium levels in whole worms, 300 synchronized L4/young adult worms were incubated for 30 min with washing buffer containing 110 mM HNO_3 (semiconductor grade, Wako) and 187 mM NH_3 (ultrapure grade, Kanto Chemical), which corresponds to approximately 300 mOsm/l and pH 7.0–8.0 at room temperature, and were then washed 5 times with washing buffer. Subsequently, worms were boiled at 95^{o}C for 5 min and sonicated using Bioruptor (UCD-250HSA; Cosmo Bio). The homogenates were completely dried by incubation at 98^{o}C, and then subjected to treatment with 100 µl of 40% HNO_3 at 95^{o}C for 2 h. The solution was diluted to 1 ml

with ddH_2O and magnesium levels were determined using ICP-MS (7700x; Agilent), according to the manufacturer's instructions. The magnesium levels were normalized to total protein levels, which were determined using the BCA assay kit (Thermo Scientific). A blank sample was prepared with same procedure without worms. For measurement of magnesium levels in the intestine, about 300 synchronized L4/young adult worms were cut with a scalpel just behind the pharynx in a drop of washing buffer. The extruded intestine was cut away from the remnants of the body, and the isolated intestines were then washed twice with washing buffer. The magnesium levels were analyzed as described above.

Volume calculation

Body volume was measured as described previously (Choe and Strange, 2007; Banerjee et al., 2015), with slight modifications. L4/young adults were transferred to M9 buffer containing 50 mM NaN_3 on coverslips, and then photographed. The total body volume of the worms was calculated by assuming that the body shape is composed of two cones (from the tip of the nose to the anterior end of the intestine, and from the posterior end of the intestine to the tip of the tail) and a cylinder (the remaining body part) and by measuring each length and radius. The volume of the intestine was calculated by assuming that its shape is cylindrical.

Microscopy

Fluorescence images were acquired using an inverted microscope (IX81; Olympus) equipped with a laser scanning confocal imaging system (FluoView FV1000; Olympus). Nomarski images were collected concurrently or alone using the same microscope using

Nomarski optics. A multiline argon laser and an image analysis system (FV10-ASW; Olympus) were also used for image acquisition. For analysis of gonadal arm extension, *lag-2p::GFP* fluorescence was observed using a stereo microscope (SZX7; Olympus) equipped with a U-RFL-T 100W mercury lamp (U-RFL-T; Olympus).

Statistics

All statistical analyses were performed using GraphPad Prism 6 software (GraphPad Software) and are presented as the mean ± SEM. *p* values were obtained by Student's two tailed t-test for Figure 8A and Table 1 and by ANOVA, followed by two tailed multiple Student's t-test with Tukey's correction for Figures 4D, 5, 7B, 7C, and 8B. For lifespan assays (Figs. 6 and 7D), I used the log rank (Mantel-Cox) test. Bonferroni correction was applied to multiple comparisons of lifespans.

Acknowledgement

I am deeply grateful to Professor Hiroaki Miki for tremendous support, helpful advice, discussion, and critical reading of my thesis. I greatly appreciate all the members of Miki Lab, especially Dr. Yosuke Funato, for technical advice and helpful discussion. I want to thank Dr. Kiyoji Nishiwaki (Kwansei Gakuin University, Japan) for providing the Trimethylpsoralen/UV-mutagenized library, Dr. Nozomu Kono and Dr. Hiroyuki Arai (Tokyo University, Japan) for providing the RNAi feeding library. I am also grateful to Dr. Andrew Fire (Stanford University, USA), Dr. Takeshi Ishihara (Kyushu University, Japan), and Dr. Hidehito Kuroyanagi (Tokyo Medical and Dental University, Japan) for their gifts of vectors. Some *C. elegans* strains used in this work were provided by the *Caenorhabditis* Genetic Centre, *C. elegans* Knockout Consortium, and NEMAGENETAG Project. I also thank Dr. Eisuke Mekada (Osaka University, Japan) and Dr. Hiroki Moribe (Kurume University, Japan) for technical advices, Dr. Yusuke Hirata (Tohoku University, Japan), Dr. Tatsuya. Hayashi, and Ms. Hiromi Yamamoto (Osaka University, Japan) for their technical assistance.

References

Al-Aidaroos, A.O., and Zeng, Q. (2010) PRL-3 phosphatase and cancer metastasis. J. Cell. Biochem. *111,* 1087–1098.

Apfeld, J., O'Connor, G., McDonagh, T., DiStefano, P.S., and Curtis, R. (2004) The AMP-activated protein kinase AAK-2 links energy levels and insulin-like signals to lifespan in C. elegans. Genes Dev. *18,* 3004–3009.

Arantes-Oliveira, N., Apfeld, J., Dillin, A., and Kenyon, C. (2002) Regulation of life-span by germ-line stem cells in Caenorhabditis elegans. Science. *295,* 502–505.

Balklava, Z., Pant, S., Fares, H., and Grant, B.D. (2007) Genome-wide analysis identifies a general requirement for polarity proteins in endocytic traffic. Nat. Cell Biol. *9,* 1066–1073.

Banerjee, S., Versaw, W.K., and Garcia, L.R. (2015) Imaging Cellular Inorganic Phosphate in Caenorhabditis elegans Using a Genetically Encoded FRET-Based Biosensor. PLoS One. *10,* e0141128.

Blelloch, R., Anna-Arriola, S.S., Gao, D., Li Y., Hodgkin, J., and Kimble, J. (1999) The gon-1 gene is required for gonadal morphogenesis in Caenorhabditis elegans. Dev. Biol. *216,* 382–393.

Brenner, S. (1974) The genetics of Caenorhabditis elegans. Genetics. *77*, 71-94.

Brooks, K.K., Liang, B., and Watts, J.L. (2009) The influence of bacterial diet on fat storage in C. elegans. PLoS One. *4*, e7545.

Castiglioni, S., Cazzaniga, A., Albisetti, W., and Maier, J.A. (2013) Magnesium and osteoporosis: Current state of knowledge and future research directions. Nutrients. *5*, 3022–3033.

Chiuve, S.E., Korngold, E.C., Januzzi, J.L., Jr., Gantzer, M.L., and Albert, C.M. (2011) Plasma and dietary magnesium and risk of sudden cardiac death in women. Am. J. Clin. Nutr. *93*, 253–260.

Choe, K.P., and Strange, K. (2007) Evolutionarily conserved WNK and Ste20 kinases are essential for acute volume recovery and survival after hypertonic shrinkage in Caenorhabditis elegans. Am. J. Physiol. Cell Physiol. *293*, C915–C927.

Cox, E.A., and Hardin, J. (2004) Sticky worms: adhesion complexes in C. elegans. J. Cell Sci. *117*, 1885–1897.

Curiel-Garcia, J.A., Rodriguez-Moran, M., and Guerrero-Romero, F. (2008) Hypomagnesemia and mortality in patients with type 2 diabetes. Magnes. Res. *21*, 163-166.

de Baaij, J.H., Stuiver, M., Meij, I.C., Lainez, S., Kopplin, K., Venselaar, H., Müller, D., Bindels, R.J., and Hoenderop, J.G. (2012) Membrane topology and intracellular processing of cyclin M2 (CNNM2). J. Biol. Chem. *287*, 13644–13655.

Dimke, H., Hoenderop, J.G., and Bindels, R.J. (2011) Molecular basis of epithelial Ca^{2+} and Mg^{2+} transport: insights from the TRP channel family. J. Physiol. *589*, 1535–1542.

Durlach, J. (1990) Magnesium depletion and pathogenesis of Alzheimer's disease. Magnes. Res. *3*, 217–218.

Edgar, L.G., and McGhee, J.D. (1986) Embryonic expression of a gut-specific esterase in Caenorhabditis elegans. Dev. Biol. *114*, 109–118.

Elin, R.J. (2010) Assessment of magnesium status for diagnosis and therapy. Magnes Res. *23*, S194-198.

Funato, Y., Yamazaki, D., Mizukami, S., Du, L., Kikuchi, K., and Miki, H. (2014) Membrane protein CNNM4-dependent Mg^{2+} efflux suppresses tumor progression. J. Clin. Invest. *124*, 5398–5410.

Gibson, M. M., Bagga, D. A., Miller, C. G., and Maguire, M. E. (1991) Magnesium transport in Salmonella typhimurium: the influence of new mutations conferring Co^{2+} resistance on the CorA Mg^{2+} transport system. Molecular Microbiology. *5*, 2753-2762.

Goytain, A., and Quamme, G.A. (2005) Functional characterization of ACDP2 (ancient conserved domain protein), a divalent metal transporter. Physiol Genomics. *22,* 382–389.

Grober, U, Schmidt, J., and Kisters, K. (2015) Magnesium in Prevention and Therapy. Nutrients. *7,* 8199-8226.

Günther, T. (2006) Concentration, compartmentation and metabolic function of intracellular free Mg^{2+}. Magnes. Res. *19,* 225–236.

Hansen, M., Flatt, T., and Aguilaniu, H. (2013) Reproduction, fat metabolism, and life span: What is the connection? Cell Metab. *17*, 10–19.

Hardie, D.G., Ross, F.A., and Hawley, S.A. (2012) AMPK: a nutrient and energy sensor that maintains energy homeostasis. Nat. Rev. Mol. Cell Biol. *13,* 251–262.

Hardy, S., Uetani, N., Wong, N., Kostantin, E., Labbé, D.P., Bégin, L.R., Mes-Masson, A., Miranda-Saavedra, D., and Tremblay, M.L. (2015) The protein tyrosine phosphatase PRL-2 interacts with the magnesium transporter CNNM3 to promote oncogenesis. Oncogene. *34*, 986-995.

Hirata, Y., Funato, Y., Takano, Y., and Miki, H. (2014) Mg^{2+}-dependent interactions of ATP with the cystathionine- β-synthase (CBS) domains of a magnesium transporter. J. Biol. Chem. *289,* 14731–14739.

Hsin, H., and Kenyon, C. (1999) Signals from the reproductive system regulate the lifespan of C. elegans. Nature. *399*, 362–366.

Hubbard, E.J., and Greenstein, D. (2000) The Caenorhabditis elegans gonad: a test tube for cell and developmental biology. Dev Dyn. *218*, 2-22.

Islam, Z., Hayashi, N., Inoue, H., Umezawa, T., Kimura, Y., Doi, H., Romero, M.F, Hirose, S., and Kato, A. (2014) Identification and lateral membrane localization of cyclin M3, likely to be involved in renal Mg^{2+} handling in seawater fish. Am J Physiol Regul Integr Comp Physiol. *307*, R525-R537.

Iwasaki, K., Staunton, J., Saifee, O., Nonet, M., and Thomas, J.H. (1997) aex-3 encodes a novel regulator of presynaptic activity in C. elegans. Neuron. *18*, 613–622.

Jshnen-Dechent, W., and Ketteler M. (2012) Magnesium basics. Clin Kidney J. *5*, i3-i14.

Kamath, R.S., Martinez-Campos, M., Zipperlen, P., Fraser, A.G., and Ahringer, J. (2001) Effectiveness of specific RNA-mediated interference through ingested double-stranded RNA in Caenorhabditis elegans. Genome Biol. *2*, RESEARCH0002.

Kamath RS, Fraser AG, Dong Y, Poulin G, Durbin R, Gotta M, et al. (2003) Systematic functional analysis of the Caenorhabditis elegans genome using RNAi. Nature. *421*, 231-237.

Kawasaki, I., Shim, Y.H., Kirchner, J., Kaminker, J., Wood, W.B., and Strome, S. (1998) PGL-1, a predicted RNA-binding component of germ granules, is essential for fertility in C. elegans. Cell. *94*, 635–645.

Kenyon, C., Chang, J., Gensch, E., Rudner, A., and Tabtiang, R. (1993) A C. elegans mutant that lives twice as long as wild type. Nature. *366*, 461–464.

Kimble, J., and Hirsh, D. (1979) The postembryonic cell lineages of the hermaphrodite and male gonads in Caenorhabditis elegans. Dev. Biol. *70*, 396–417.

Kimura, K.D., Tissenbaum, H.A., Liu, Y., and Ruvkun, G. (1997) daf-2, an insulin receptor-like gene that regulates longevity and diapause in Caenorhabditis elegans. Science. *277*, 942-946.

Kubota, Y., Kuroki, R., and Nishiwaki, K. (2004) A fibulin-1 homolog interacts with an ADAM protease that controls cell migration in C. elegans. Curr. Biol. *14*, 2011–2018.

Kuroyanagi, H., Kobayashi, T., Mitani, S., and Hagiwara, M. (2006) Transgenic alternative-splicing reporters reveal tissue-specific expression profiles and regulation mechanisms in vivo. Nat. Methods. *3*, 909–915.

Kuroyanagi, H., Ohno, G., Sakane, H., Maruoka, H., and Hagiwara, M. (2010) Visualization and genetic analysis of alternative splicing regulation in vivo using

fluorescence reporters in transgenic Caenorhabditis elegans. Nat. Protoc. *5*, 1495–1517.

Larsson, S.C., Orsini, N., and Wolk, A. (2012) Dietary magnesium intake and risk of stroke: A meta-analysis of prospective studies. Am. J. Clin. Nutr. *95*, 362–366.

Mathies, L.D., Schvarzstein, M., Morphy, K.M., Blelloch, R., Spence, A.M., and Kimble, J. (2004) TRA-1/GLI controls development of somatic gonadal precursors in C. elegans. Development. *131*, 4333-4343.

Mello, C.C., Kramer, J.M., Stinchcomb, D., and Ambros, V. (1991) Efficient gene transfer in C.elegans: extrachromosomal maintenance and integration of transforming sequences. EMBO J. *10*, 3959–3970.

Meyer, T.E., Verwoert, G.C., Hwang, S.J., Glazer, N.L., Smith, A.V, van Rooij, F.J., Ehret, G.B., Boerwinkle, E., Felix, J.F., Leak, T.S., et al. (2010) Genome-wide association studies of serum magnesium, potassium, and sodium concentrations identify six Loci influencing serum magnesium levels. PLoS Genet. *6*, e1001045.

Nielsen, F.H. (2010) Magnesium, inflammation, and obesity in chronic disease. Nutr Rev. *68*, 333–340.

Ogg, S., Paradis, S., Gottlieb, S., Patterson, G.I., Lee, L., Tissenbaum, H.A., and Ruvkun, G. (1997) The Fork head transcription factor DAF-16 transduces insulin-like metabolic and longevity signals in C. elegans. Nature. *389*, 994-999.

O'Rourke, E.J., Soukas, A.A., Carr, C.E., and Ruvkun, G. (2009) C. elegans major fats are stored in vesicles distinct from lysosome-related organelles. Cell Metab. *10*, 430-435.

Parry, D.A., Mighell, A.J., El-Sayed, W., Shore, R.C., Jalili, I.K., Dollfus, H., Bloch-Zupan, A., Carlos, R., Carr, I.M., Downey, L.M., Blain, K.M., Mansfield, D.C., Shahrabi, M., Heidari, M., Aref, P., Abbasi, M., Michaelides, M., Moore, A.T., Kirkham, J., and Inglehearn, C.F. (2009) Mutations in CNNM4 cause Jalili syndrome, consisting of autosomal-recessive cone-rod dystrophy and amelogenesis imperfecta. Am J Hum Genet. *84*, 266–273.

Polo, S., and Di Fiore, P.P. (2006) Endocytosis conducts the cell signaling orchestra. Cell. *124*, 897–900.

Polok, B., Escher, P., Ambresin, A., Chouery, E., Bolay, S., Meunier, I., Nan, F., Hamel, C., Munier, F.L., Thilo, B., garbane, A.M., and Schorderet, D.F. (2009) Mutations in CNNM4 cause recessive cone-rod dystrophy with amelogenesis imperfecta. Am J Hum Genet. *84*, 259–265.

Rios, P., Li, X., and Köhn, M. (2013) Molecular mechanisms of the PRL phosphatases. FEBS J. *280*, 505–524.

Romani, A.M. (2011) Cellular magnesium homeostasis. Arch. Biochem. Biophys. *512*,

1–23.

Rosanoff, A., and Plesset, M.R. (2013) Oral magnesium supplements decrease high blood pressure (SBP > 155 mm Hg) in hypertensive subjects on anti-hypertensive medications: A targeted meta-analysis. Magnes. Res. *26*, 93–99.

Rubin, H. (1975) Central role for magnesium in coordinate control of metabolism and growth in animal cells. Proc. Natl. Acad. Sci. U. S. A. *72*, 3551–3555.

Rubin, H. (2007) The logic of the Membrane, Magnesium, Mitosis (MMM) model for the regulation of animal cell proliferation. Arch. Biochem. Biophys. *458*, 16-23.

Ryazanova, L.V., Rondon, L.J., Zierler, S., Hu, Z., Galli, J., Yamaguchi, T.P., Mazur, A., Fleig, A., and Ryazanov, A.G. (2010) TRPM7 is essential for Mg(2+) homeostasis in mammals. Nat. Commun. *1*, 109.

Sahni, J., Scharenberg, A.M. (2008) TRPM7 ion channels are required for sustained phosphoinositide 3-kinase signaling in lymphocytes. Cell Metab. *8*, 84–93.

Schlingmann, K.P., Weber, S., Peters, M., Niemann Nejsum, L., Vitzthum, H., Klingel, K., Kratz, M., Haddad, E., Ristoff, E., Dinour, D., et al. (2002) Hypomagnesemia with secondary hypocalcemia is caused by mutations in TRPM6, a new member of the TRPM gene family. Nat. Genet. *31*, 166–170.

Schweigel, M., and Martens, H. (2000) Magnesium transport in the gastrointestinal tract. Front. Biosci. *5*, D666–D677.

Shah, N.C., Shah, J.G., Li, Z., Jiang, X.C., Altura, B.T., and Altura, B.M. (2014) Short-term magnesium deficiency downregulates telomerase, upregulates neutral sphingomyelinase and induces oxidative DNA damage in cardiovascular tissues: relevance to atherogenesis, cardiovascular diseases and aging. Int. J. Clin. Exp. Med. *7*, 497–514.

Sharma-Kishore, R., White, J.G., Southgate, E., and Podbilewicz, B. (1999) Formation of the vulva in Caenorhabditis elegans: a paradigm for organogenesis. Development. *126*, 691–699.

Simmer, F., Moorman, C., van der Linden, A.M., Kuijk, E., van den Berghe, P.V., Kamath, R.S., Fraser, A.G., Ahringer, J., and Plasterk, R.H. (2003) Genome-wide RNAi of C. elegans using the hypersensitive rrf-3 strain reveals novel gene functions. PLoS Biol. *1*, E12.

Singh, R.N., and Sulston, J.E. (1978) Some Observations On Moulting in Caenorhabditis Elegans. Nematologica. *24*, 63–71.

Sorkin, A., and von Zastrow, M. (2009) Endocytosis and signalling: intertwining molecular networks. Nat. Rev. Mol. Cell Biol. *10*, 609–622.

Srinivasan, S., Sadegh, L., Elle, I.C., Christensen, A.G., Faergeman, N.J., and Ashrafi, K. (2008) Serotonin regulates C. elegans fat and feeding through independent molecular mechanisms. Cell Metab. *7,* 533-544.

Strome, S., and Wood, W.B. (1983) Generation of asymmetry and segregation of germ-line granules in early C. elegans embryos. Cell. *35*, 15–25.

Stuiver, M., Lainez, S., Will, C., Terryn, S., Günzel, D., Debaix, H., Sommer, K., Kopplin, K., Thumfart, J., Kampik, N.B., et al. (2011) CNNM2, encoding a basolateral protein required for renal Mg^{2+} handling, is mutated in dominant hypomagnesemia. Am. J. Hum. Genet. *88*, 333–343.

Sulston, J.E., and Horvitz, H.R. (1977) Post-embryonic cell lineages of the nematode, Caenorhabditis elegans. Dev. Biol. *56*, 110–156.

Sulston, J.E., Schierenberg, E., White, J.G., and Thomson, J.N. (1983) The embryonic cell lineage of the nematode Caenorhabditis elegans. Dev Biol. *100,* 64-119.

Sun, A.Y., and Lambie, E.J. (1997) gon-2, a gene required for gonadogenesis in Caenorhabditis elegans. Genetics. *147,* 1077–1089.

Tabara, H., Grishok, A., and Mello, C.C. (1998) RNAi in C. elegans: soaking in the genome sequence. Science. *282,* 430-431.

Teramoto, T., Lambie, E.J., and Iwasaki, K. (2005) Differential regulation of TRPM channels governs electrolyte homeostasis in the C. elegans intestine. Cell Metab. *1*, 343–354.

Teramoto, T., Sternick, L.A., Kage-Nakadai, E., Sajjadi, S., Siembida, J., Mitani, S., Iwasaki, K., and Lambie, E.J. (2010) Magnesium Excretion in C. elegans Requires the Activity of the GTL-2 TRPM Channel. PLoS One. *5*, e9589.

Timmons, L., and Fire, A. (1998) Specific interference by ingested dsRNA. Nature. *395*, 854.

Traub, L.M. (2009) Tickets to ride: selecting cargo for clathrin-regulated internalization. Nat. Rev. Mol. Cell Biol. *10*, 583–596.

Vallin, E., Gallagher, J., Granger, L., Martin, E., Belougne, J., Maurizio, J., Duverger, Y., Scaglione, S., Borrel, C., Cortier, E., et al. (2012) A genome-wide collection of Mos1 transposon insertion mutants for the C. elegans research community. PLoS One. *7*, e30482.

Voets, T., Nilius, B., Hoefs, S., van der Kemp, A.W., Droogmans, G., Bindels, R.J., and Hoenderop, J.G. (2004) TRPM6 Forms the Mg^{2+} Influx Channel Involved in Intestinal and Renal Mg^{2+} Absorption. J. Biol. Chem. *279*, 19–25.

Walder, R.Y., Landau, D., Meyer, P., Shalev, H., Tsolia, M., Borochowitz, Z., Boettger,

M.B., Beck, G.E., Englehardt, R.K., Carmi, R., and Sheffield, V.C. (2002) Mutation of TRPM6 causes familial hypomagnesemia with secondary hypocalcemia. Nat. Genet. *31*, 171–174.

Wang, C.Y., Shi, J.D., Yang, P., Kumar, P.G., Li, Q.Z., Run, Q.G., Su, Y.C., Scott, H.S., Kao, K.J., and She, J.X. (2003) Molecular cloning and characterization of a novel gene family of four ancient conserved domain proteins (ACDP). Gene. *306*, 37–44.

Yamazaki, D., Funato, Y., Miura, J., Sato, S., Toyosawa, S., Furutani, K., Kurachi, Y., Omori, Y., Furukawa, T., Tsuda, T., et al. (2013) Basolateral Mg^{2+} extrusion via CNNM4 mediates transcellular Mg^{2+} transport across epithelia: a mouse model. PLoS Genet. *9*, e1003983.

Yen, K., Le, T.T., Bansal, A., Narasimhan, S.D., Cheng, J.X., and Tissenbaum, H.A. (2010) A comparative study of fat storage quantitation in nematode Caenorhabditis elegans using label and label-free methods. PLoS One. *5*, e12810.

Figure legends

Figure 1. Sequence characteristics of the CNNM family

(A) Schematic illustrations of the CNNM family proteins. Yellow, DUF21 domains; blue, CBS domains; green, sequence motifs present in the cyclin box; purple, cyclic nucleotide monophosphate binding domains. (B) Sequence alignment of DUF21 and CBS domains of CNNM proteins from the following species (NCBI protein database accession numbers are shown in parentheses): *Homo sapiens* CNNM4 (NP_064569.3), *Mus musculus* CNNM4 (NP_291048.2), *Gallus gallus* CNNM4 (XP_003643479.2), *Danio rerio* CNNM4 (XP_009299521.1), *Drosophila melanogaster* Unextended (NP_001104391.2), *Caenorhabditis elegans* CNNM-1 (NP_503052.1), *Saccharomyces cerevisiae* Mam3p (AJU02166.1), and *Shewanella oneidensis* CorC (WP_011071563.1). The alignment was constructed using Clustal Omega and GeneDoc. Residues are grouped based on the chemical property and then residues with similar chemical property in all eight, seven, and six species are shaded in dark, dark gray, and light gray, respectively.

Figure 2. Lifecycle and gonadogenesis of *C. elegans* hermaphrodites

(A) The newly hatched larvae grow and molt through 4 larval stages (L1–L4), maturing into the egg-laying adults. The average time intervals between the stages grown at 20 ^{o}C are indicated. (B) Schematic illustrations of gonad at the indicated stages are shown. Blue, germ cells; red, DTCs; gray, embryos.

Figure 3. Gene structure of the *C. elegans cnnm* family

Schematic illustrations of the *C. elegans cnnm* family genes. Exons and introns are indicated by boxes and lines, respectively. The regions encoding the evolutionarily conserved DUF21 and CBS domains are indicated by black and gray boxes, respectively. Sequence names are shown in parentheses. The illustrations were generated using the Exon-Intron Graphic Maker by Nikhil Bhatla (http://www.wormweb.org/exonintron). Lines, deletion; arrowhead, point mutation; arrow, *Mos1* insertion.

Figure 4. Mutations in *cnnm-1* and *cnnm-3* cause sterility, decrease body size, and retards growth

(A) Quantification of the sterile phenotype for each genotype. Eggs collected by synchronous laying were grown for 4 days and then examined for the presence of embryos in their uteri by microscopic observation. Worms lacking embryos were scored as sterile. More than 100 worms were analyzed for each genotype. (B) Nomarski images of wild-type and *cnnm-1; cnnm-3* mutant worms grown for 3 days. The high magnification views of the boxed areas are also shown (right). The arrow indicates the vulva. Bar, 30 μm. (C) Nomarski images of wild-type L4 larva (left) and adult (right) worms are shown. Dotted lines indicate the outlines of the alae. Bar, 5 μm. (D) Mixed stage worms from L2 to adult (L4 to adult worms comprise the most) were examined for alae formation and subjected to body size measurement (n = 30 per each experiment). The body size at the transition from L4 to the adult molt was estimated by calculating the mean body size of the smallest three worms with alae and the largest three worms without alae. The data are shown as the means of three experiments. Error bars indicate SEM. p values were determined by ANOVA, followed by two tailed

multiple Student's t-test with Tukey's correction. *p < 0.05. (E) Eggs collected by synchronous laying were grown at 20°C and examined for alae formation using a microscope at the indicated time points (n = 10 per each time point). The data are shown as the means of three experiments. Error bars indicate SEM.

Figure 5. Mutations in *cnnm-1* and *cnnm-3* increase fat storage

Day 3 adult worms of the indicated genotype were fixed and stained with Nile Red, followed by measurement of their fluorescence intensity (bottom right). The data are shown as the means of at least three experiments (n = 10–15 for each experiment). Error bars indicate SEM. p values were determined by ANOVA, followed by two tailed multiple Student's t-tests with Tukey's correction. *p < 0.05. Bar, 100 μm.

Figure 6. Mutations in *cnnm-1* and *cnnm-3* shorten life span

Lifespan of worms of the indicated genotype. For each genotype, 45 synchronized L4/young adult worms were transferred to fresh plates (15 worms per plate), and were then scored daily for survival. The graph represents data combined from at least two experiments. Mean lifespan (± SEM) of worms is also indicated in parentheses. p values were determined by log rank (Mantel-Cox) test, and Bonferroni method was then used to correct for multiple comparisons. ****p < 0.0001.

Figure 7. Effects of Mg^{2+} supplementation on *cnnm-1; cnnm-3* mutant worms

(A) *cnnm-1; cnnm-3* mutant worms were grown on plates supplemented with the indicated concentrations of Mg^{2+} or Ca^{2+} for 4 days and then examined for sterility. More than 50 worms were analyzed for each experimental condition. (B) Quantitative

analysis of Nile Red staining. Day 3 adult worms of the indicated genotype grown on plates supplemented with 1 mM Mg^{2+} or Ca^{2+} were fixed and stained with Nile Red, followed by measurement of their fluorescence intensity. The data are shown as the means of at least two experiments (n = 10–15 per experiment). Error bars indicate SEM. p values were determined by ANOVA, followed by two tailed multiple Student's t-tests with Tukey's correction. *$p < 0.05$. (C) Wild-type and *cnnm-1; cnnm-3* mutant worms were grown on plates supplemented with 1 mM Mg^{2+} or Ca^{2+} for at least two generations. Mixed stage worms from L2 to adult (L4 to adult worms comprise the most) were examined for alae formation and subjected to body size measurement (n = 30 per each experiment). Body size at the transition from L4 to adult molt was estimated as in Fig. 4D. The data are shown as the means of three experiments. Error bars indicate SEM. p values were determined by ANOVA, followed by two tailed multiple Student's t-tests with Tukey's correction. *$p < 0.05$. (D) 45 synchronized L4/young adult worms of the indicated genotype were transferred to fresh plates supplemented with 1 mM Mg^{2+} or Ca^{2+} (15 worms per plate), and then scored for survival daily. The graph represents data combined from at least two experiments. Mean lifespan (± SEM) of worms is also indicated in parentheses. p values were determined by log rank (Mantel-Cox) test, and Bonferroni method was then used to correct for multiple comparisons. ****$p < 0.0001$.

Figure 8. Dysregulation of DAF-16 or alteration of food intake are not responsible for the increased fat storage in *cnnm-1; cnnm-3* mutants

(A) L4/young adult worms were examined for the pharyngeal pumping rate. The data are shown as the means of two experiments (n = 10 per experiment). Error bars indicate

SEM. *p* value was determined by two tailed Student's t-tests. (B) Day 3 adult worms of the indicated genotype were fixed and stained with Nile Red, followed by measurement of their fluorescence intensity (bottom). The data are shown as the means of two experiments (n = 10–15 for each experiment). Error bars indicate SEM. *p* values were determined by ANOVA, followed by two tailed multiple Student's t-tests with Tukey's correction. $*p < 0.05$. Bar, 100 μm.

Figure 9. *cnnm-1* and *cnnm-3* are required for postembryonic development of the gonad

(A) L4/young adult worms of the indicated genotype, carrying *lag-2p::GFP*, were examined for gonadal arm extension. Representative images and the high magnification view of the boxed area are shown (left). In each image, the anterior side of the worm is positioned to the left. Dotted lines indicate the outlines of the gonad. Bar, 20 μm. Worms with gonads of ≧ 60 μm in length of the long axis (3-fold as long as the primordial gonad) were determined as extended and the results (%) are shown in the graph (right). More than 100 worms were analyzed. (B) The worms were stained with DAPI (blue) and anti-PGL-1 antibody (red), and then the number of germ cells (PGL-1 positive cells) per worm was counted. Representative images and the high magnification view of the boxed area are shown (top). Bar, 15 μm. The graph indicates the distribution of worms (%) with the indicated numbers of germ cells (bottom).

Figure 10. Localization of CNNM-1 at the basolateral membrane of the intestinal cells

(A) Fluorescent images of wild-type L1 larvae with *cnnm-1p::GFP* or *cnnm-3p::GFP*.

Bar, 30 μm. (B) Quantification of sterile phenotype in wild-type, *cnnm-1; cnnm-3* mutants, and *cnnm-1; cnnm-3* mutants expressing CNNM-1 in the intestine (*ges-1p*) or in the pan-neuron (*aex-3p*). More than 50 worms were analyzed for each genotype. (C) Fluorescent images of intestinal cells from wild-type L1 larvae expressing the Venus-fusion proteins of CNNM-1 (left). Schematic representation of the intestinal cell plasma membranes (right). Apical and basolateral membranes are indicated by dotted and solid lines, respectively. Bar, 10 μm. (D) Regulatory model of Mg^{2+} levels in intestinal (int.) cells and in the pseudocoelom (pc) of wild-type (left) and *cnnm-1; cnnm-3* mutant (right) worms. Expected concentrations of Mg^{2+} are indicated as the pseudo-colored image.

Figure 11. Representative images showing the effect of RNAi screening.

Representative images of L4/young adult worms of *cnnm-1; cnnm-3; rrf-3* mutants with *Ex[lag-2p::GFP]*, which were fed with bacteria carrying the dsRNA corresponding to the indicated genes (the results of the top 5 genes in second round screening are shown). In each image, the anterior side of the worm is positioned to the left. Dotted lines indicate the outlines of the gonad. As a negative control, the worms were fed with bacteria carrying the empty vector L4440. Bar, 20 μm.

Figure 12. AMPK mediates the gonadogenesis defect of *cnnm-1; cnnm-3* mutant worms

(A) L4/young adult worms of the indicated genotype, carrying *lag-2p::GFP*, were examined for gonadal arm extension. Representative images are shown (left). In each image, the anterior side of the worm is positioned to the left. Dotted lines indicate the

outlines of the gonad. Bar, 20 μm. Worms with gonad of ≧60 μm in length of the long axis (3-fold as long as the primordial gonad) were determined as extended and the results (%) are shown in the graph (right). More than 100 worms were analyzed. (B) *cnnm-1; cnnm-3; aak-1; aak-2* mutant worms were stained with DAPI (blue) and anti-PGL-1 antibody (red), and then the number of germ cells (PGL-1 positive cells) per worm was counted. Representative images are shown (left). Bar, 15 μm. The graph indicates the distribution of worms (%) with the indicated numbers of germ cells (right).

Table 1

	Wild-type	*cnnm-1; cnnm-3*	*p*-value
Total (ppb/µg)	3.9 ± 0.2	5.6 ± 0.4	0.014
Intestine (ppb/µg)	4.0 ± 0.4	7.8 ± 0.8	0.015
Other tissues (ppb/µg)(estimated value)	3.9	2.6	ND

Table 1. Magnesium levels in wild-type and *cnnm-1; cnnm-3* mutant worms

The total and intestinal levels of magnesium were directly determined by ICP-MS using L4/young adult worms. The data are shown as the means (± SEM) of three experiments. Magnesium levels in the other remaining tissues were estimated by calculating the total body volume (wild-type: 1,170 ± 61 nl, n = 10; *cnnm-1; cnnm-3*: 638 ± 38 nl, n = 10) and intestine (wild-type: 458 ± 22 nl, n = 10; *cnnm-1; cnnm-3*: 357 ± 13 nl, n = 10). p values were determined by Student's two tailed t-test.

Table 2

			(%) gonadal arm extended	
Sequence name	**Gene name**	**Description**	**1st round**	**2nd round**
C10E2.6	*mct-6*	Monocarboxylate transporter	100	100
R160.1	*dpy-23*	AP-2 complex subunit mu2	100	100
C06B8.7		Scavenger receptor cysteine-rich domain	100	100
F55D10.3	*glit-1*	Thyroglobulin	80	93
T05H4.5	*hpo-19*	NADH-cytochrome b5 reductase	90	90
C55B7.8	*dbr-1*	RNA-lariat debranching enzyme	90	87
F02E8.3	*aps-2*	AP-2 complex subunit sigma2	90	87
T01C8.1	*aak-2*	AMPK alpha2	80	87
C34C6.6	*prx-5*	Peroxisomal targeting signal 1 receptor	80	87
R03E1.1	*sym-4*	WD repeat-containing protein	80	83
F29A7.6		M-phase phosphoprotein 6	100	83
T14G10.7	*hpo-5*	GPI transamidase component PIG-S	70	83
C07A9.11	*ncx-7*	Sodium/potassium/calcium exchanger	90	80
R12C12.2	*ran-5*	RanBP1 domain	80	77
F11E6.5	*elo-2*	palmitic acid elongase	50	73
F36H12.5		Transcription initiation factor TFIID subunit 3	80	73
F44A6.2	*sex-1*	Nuclear hormone receptor	60	73
F58B3.4		Nucleolar pre-rRNA processing protein	80	70
C27F2.8		Transmembrane protein 131	80	67
T26A8.4		Zinc finger CCCH domain-containing protein 4	80	67
K04E7.2	*pept-1*	Oligopeptide transporter	80	67
Y65B4BR.4	*wwp-1*	NEDD4-like E3 ubiquitin-protein ligase WWP1	50	63
C09H6.3	*mau-2*	MAU2 chromatid cohesion factor homolog	70	60
C27B7.8	*rap-1*	Ras-related protein Rap-1b	50	60
F23C8.6	*did-2*	Charged multivesicular body protein 1b	50	57
F08B12.2	*prx-12*	Peroxisomal biogenesis factor 12	60	57
ZK418.4	*lin-37*	LIN37 family protein	70	53
R07H5.8		Adenosine kinase	60	53
Y71H10B.1		Cytosolic purine 5'-nucleotidase	50	53
Y40B1B.7		Coiled-coil domain-containing protein 86	50	53
F46F11.4	*ubl-5*	Ubiquitin-like protein 5	50	50

Table 2. Genes of which RNAi suppressed the gonadogenesis defect in *cnnm-1; cnnm-3* mutant worms

Genome wide RNAi screening identified 31 genes that functionally associate with *cnnm-1* and *cnnm-3*. This information is derived from either Wormbase or InterProScan.

Figure 1

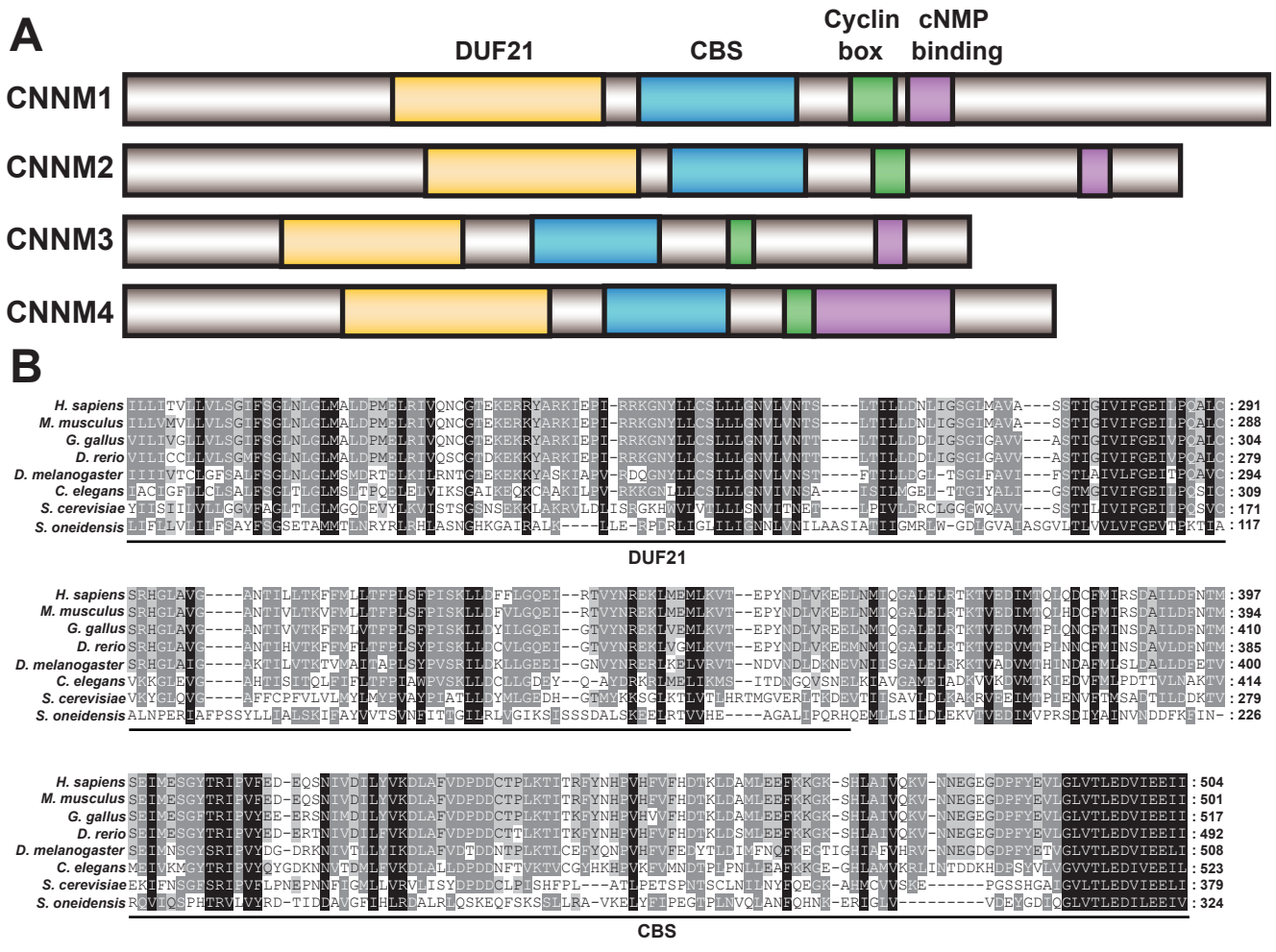
A
DUF21
CBS
Cyclin box
cNMP binding
CNNM1
CNNM2
CNNM3
CNNM4
B
H. sapiens
M. musculus
G. gallus
D. rerio
D. melanogaster
C. elegans
S. cerevisiae
S. oneidensis
DUF21
CBS

Figure 2

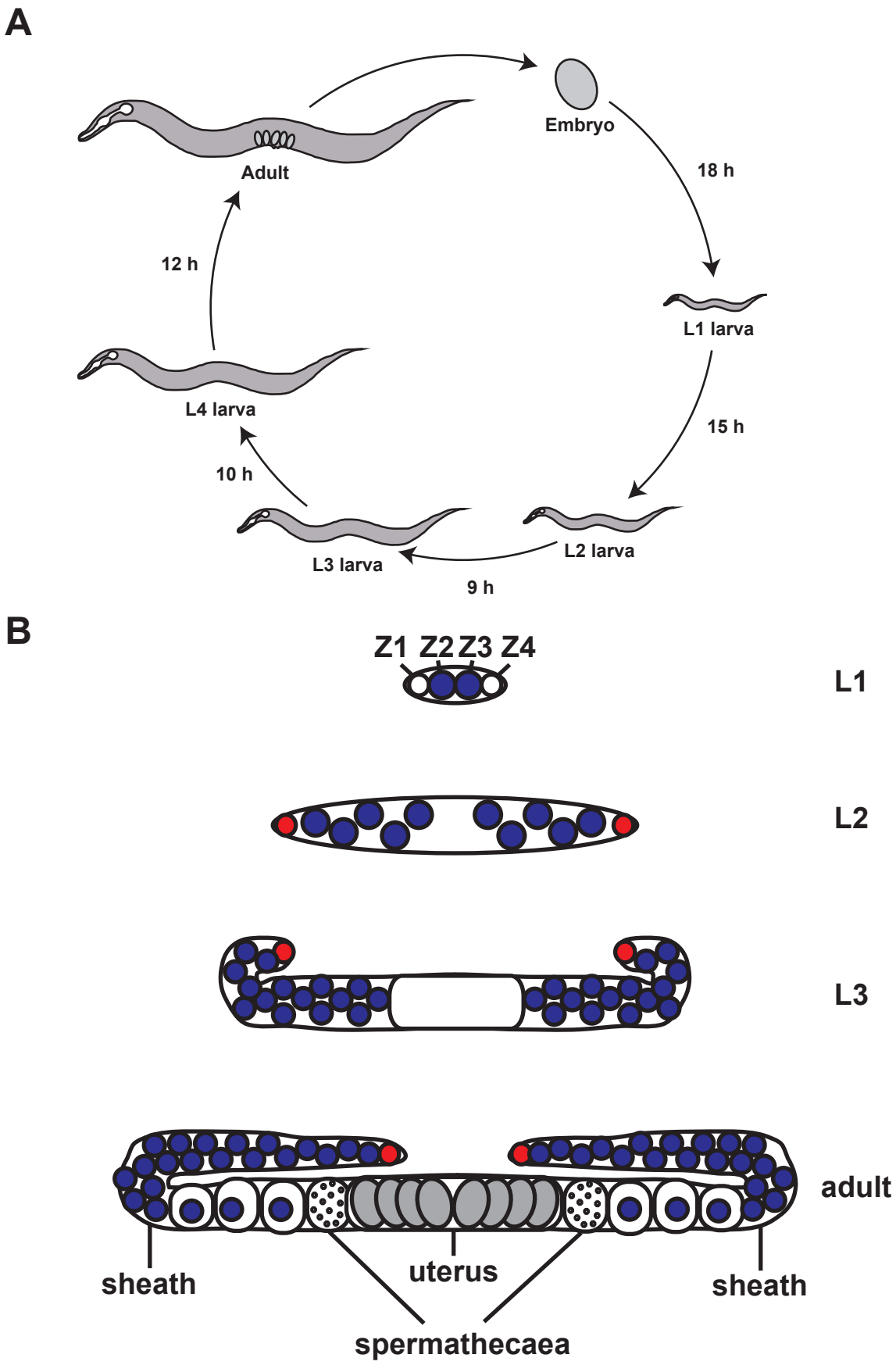
A
Embryo
18 h
L1 larva
15 h
L2 larva
9 h
L3 larva
10 h
L4 larva
12 h
Adult
B
Z1 Z2 Z3 Z4
L1
L2
L3
adult
sheath
uterus
sheath
spermathecaea

Figure 3

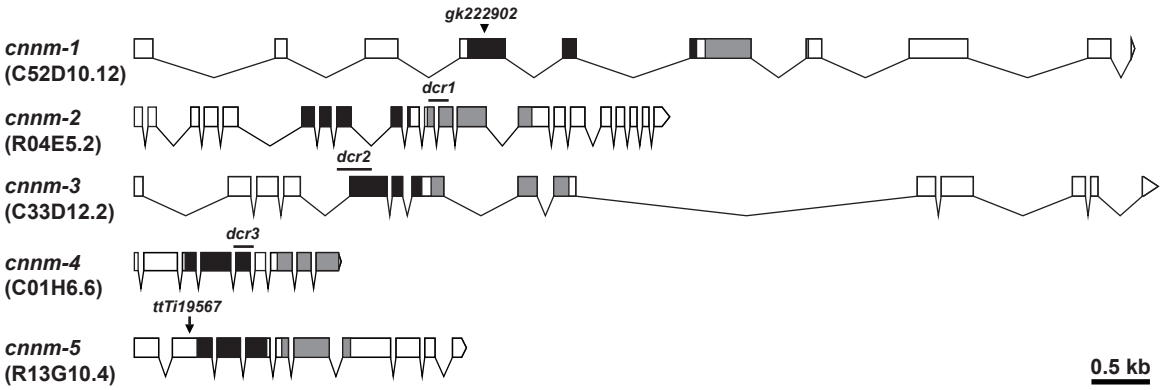
gk222902
cnnm-1
(C52D10.12)
dcr1
cnnm-2
(R04E5.2)
dcr2
cnnm-3
(C33D12.2)
dcr3
cnnm-4
(C01H6.6)
ttTi19567
cnnm-5
(R13G10.4)
0.5 kb

Figure 4

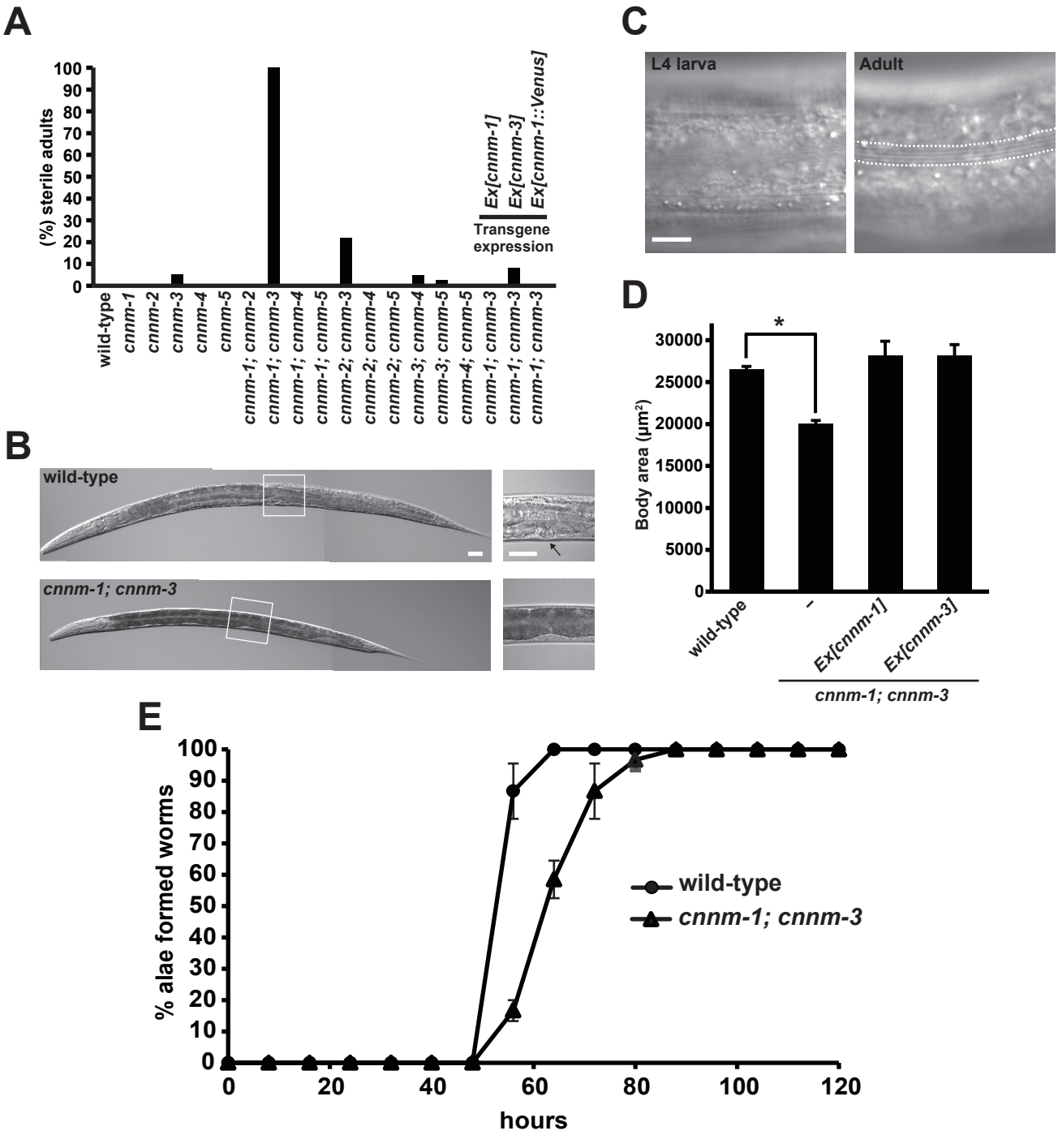
A
(%) sterile adults
100
90
80
70
60
50
40
30
20
10
0
wild-type
cnnm-1
cnnm-2
cnnm-3
cnnm-4
cnnm-5
cnnm-1; cnnm-2
cnnm-1; cnnm-3
cnnm-1; cnnm-4
cnnm-1; cnnm-5
cnnm-2; cnnm-3
cnnm-2; cnnm-4
cnnm-2; cnnm-5
cnnm-3; cnnm-4
cnnm-3; cnnm-5
cnnm-4; cnnm-5
cnnm-1; cnnm-3
cnnm-1; cnnm-3
cnnm-1; cnnm-3
Ex[cnnm-1]
Ex[cnnm-3]
Ex[cnnm-1::Venus]
Transgene expression
B
wild-type
cnnm-1; cnnm-3
C
L4 larva
Adult
D
Body area (μm²)
30000
25000
20000
15000
10000
5000
0
*
wild-type
–
Ex[cnnm-1]
Ex[cnnm-3]
cnnm-1; cnnm-3
E
% alae formed worms
100
90
80
70
60
50
40
30
20
10
0
0
20
40
60
80
100
120
hours
wild-type
cnnm-1; cnnm-3

Figure 5

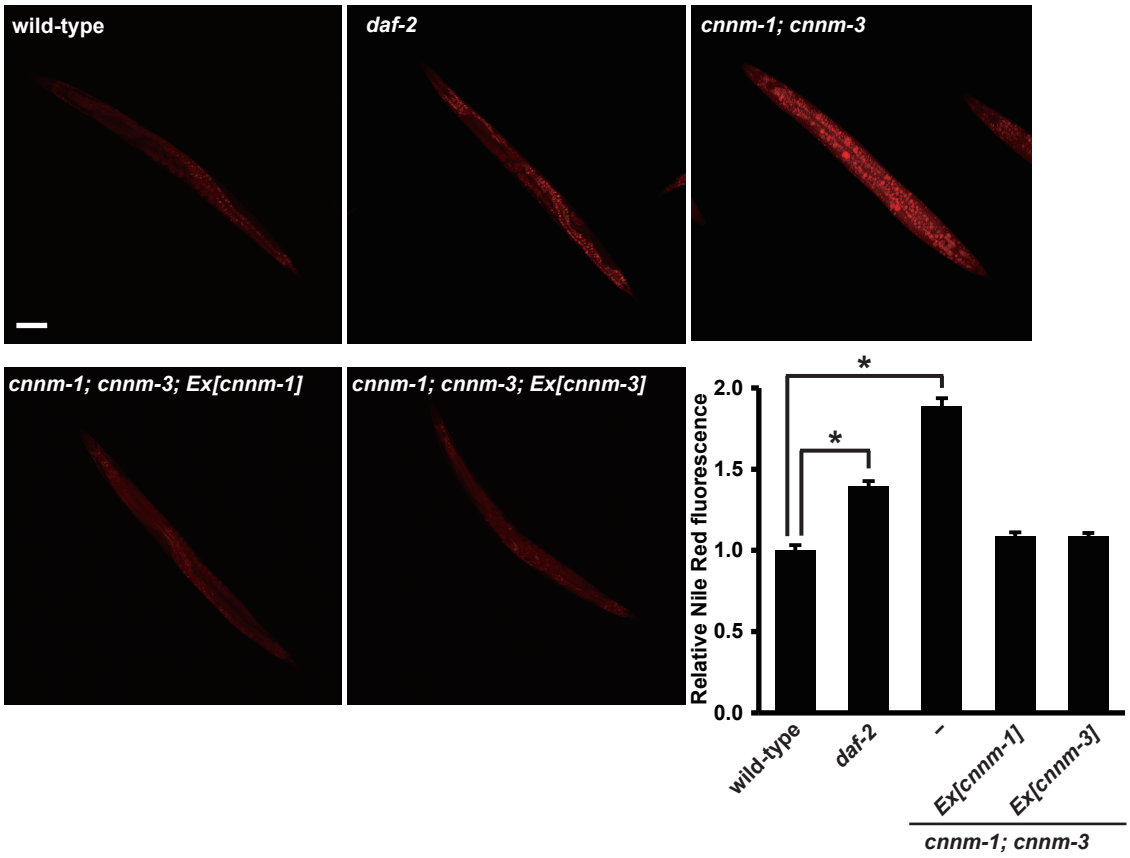
wild-type
daf-2
cnnm-1; cnnm-3
cnnm-1; cnnm-3; Ex[cnnm-1]
cnnm-1; cnnm-3; Ex[cnnm-3]
Relative Nile Red fluorescence
2.0
1.5
1.0
0.5
0.0
*
*
wild-type
daf-2
–
Ex[cnnm-1]
Ex[cnnm-3]
cnnm-1; cnnm-3

Figure 6

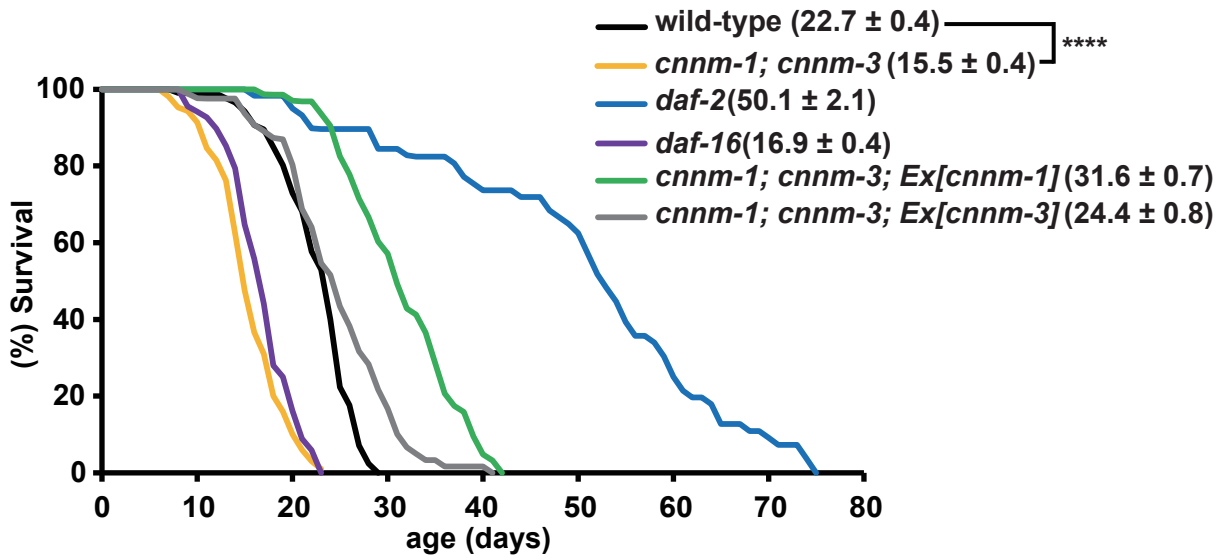
wild-type (22.7 ± 0.4)
cnnm-1; cnnm-3 (15.5 ± 0.4)
****
daf-2(50.1 ± 2.1)
daf-16(16.9 ± 0.4)
cnnm-1; cnnm-3; Ex[cnnm-1] (31.6 ± 0.7)
cnnm-1; cnnm-3; Ex[cnnm-3] (24.4 ± 0.8)
(%) Survival
100
80
60
40
20
0
0
10
20
30
40
50
60
70
80
age (days)

Figure 7

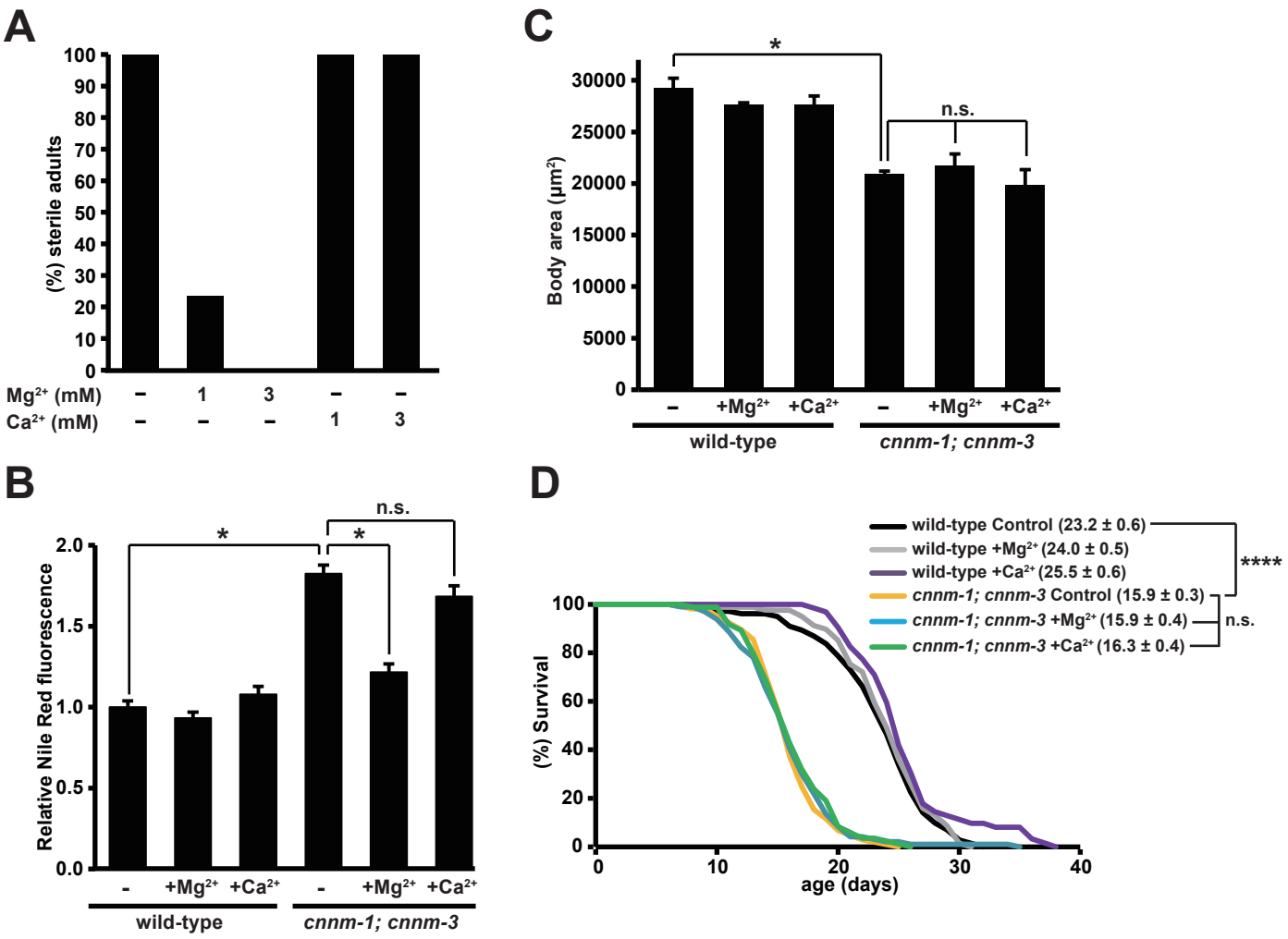
A
(%) sterile adults
100
90
80
70
60
50
40
30
20
10
0
Mg2+ (mM) – 1 3 – –
Ca2+ (mM) – – – 1 3
B
Relative Nile Red fluorescence
2.0
1.5
1.0
0.5
0.0
*
*
n.s.
- +Mg2+ +Ca2+ - +Mg2+ +Ca2+
wild-type
cnnm-1; cnnm-3
C
Body area (µm2)
30000
25000
20000
15000
10000
5000
0
*
n.s.
– +Mg2+ +Ca2+ – +Mg2+ +Ca2+
wild-type
cnnm-1; cnnm-3
D
(%) Survival
100
80
60
40
20
0
0
10
20
30
40
age (days)
wild-type Control (23.2 ± 0.6)
wild-type +Mg2+ (24.0 ± 0.5)
wild-type +Ca2+ (25.5 ± 0.6)
cnnm-1; cnnm-3 Control (15.9 ± 0.3)
cnnm-1; cnnm-3 +Mg2+ (15.9 ± 0.4)
cnnm-1; cnnm-3 +Ca2+ (16.3 ± 0.4)
****
n.s.

Figure 8

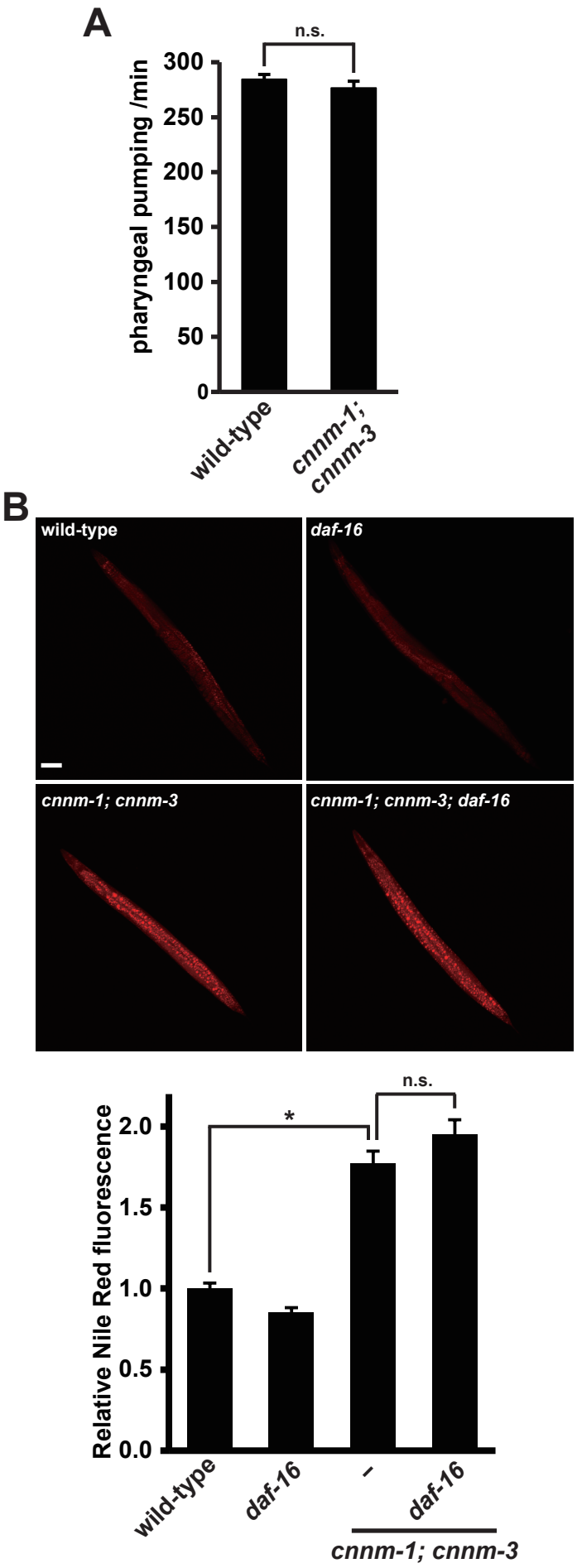
A
n.s.
pharyngeal pumping /min
300
250
200
150
100
50
0
wild-type
cnnm-1; cnnm-3
B
wild-type
daf-16
cnnm-1; cnnm-3
cnnm-1; cnnm-3; daf-16
n.s.
*
Relative Nile Red fluorescence
2.0
1.5
1.0
0.5
0.0
wild-type
daf-16
-
daf-16
cnnm-1; cnnm-3

Figure 9

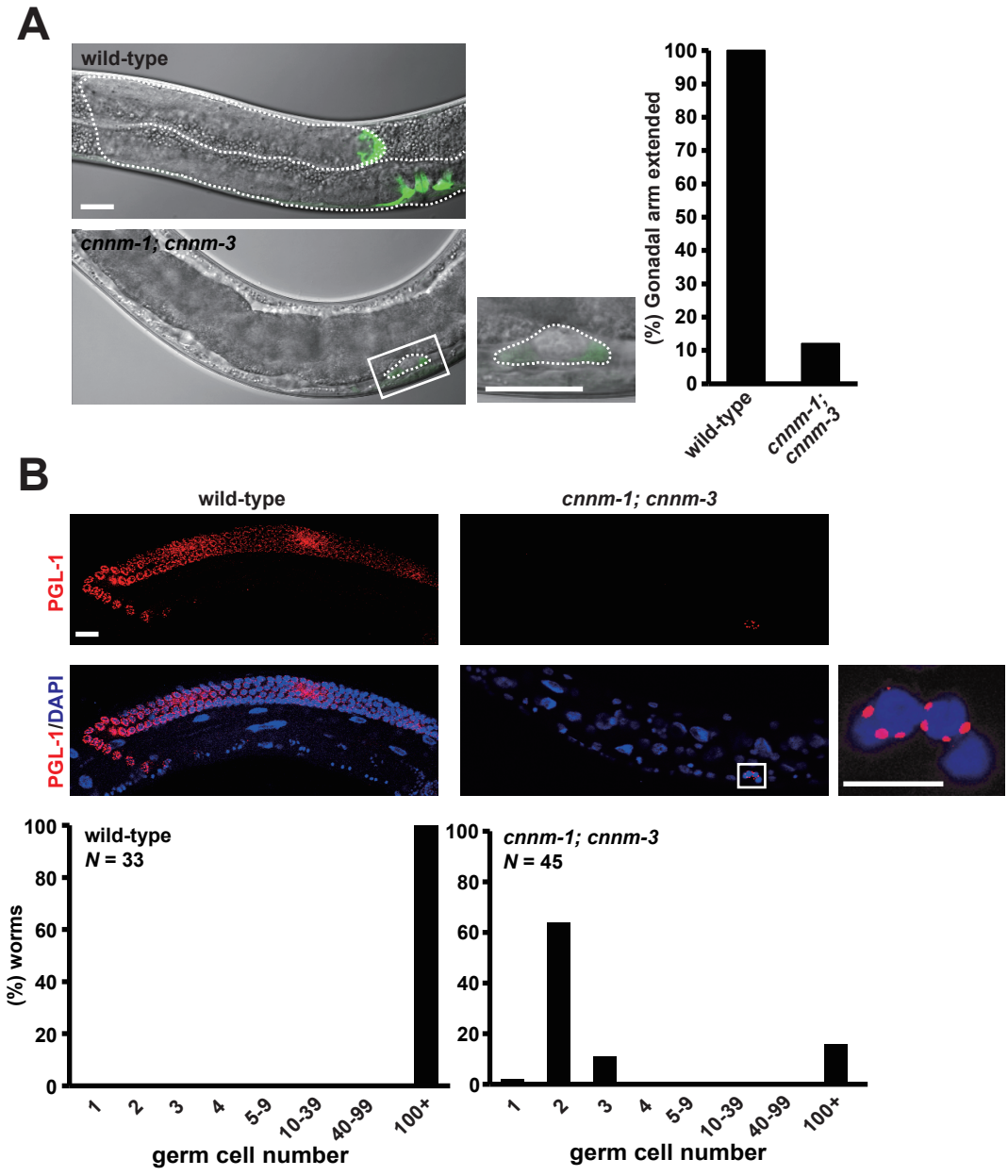
A
wild-type
cnnm-1; cnnm-3
(%) Gonadal arm extended
100
90
80
70
60
50
40
30
20
10
0
wild-type
cnnm-1; cnnm-3
B
wild-type
cnnm-1; cnnm-3
PGL-1
PGL-1/DAPI
wild-type
N = 33
cnnm-1; cnnm-3
N = 45
(%) worms
100
80
60
40
20
0
1
2
3
4
5-9
10-39
40-99
100+
germ cell number

Figure 10

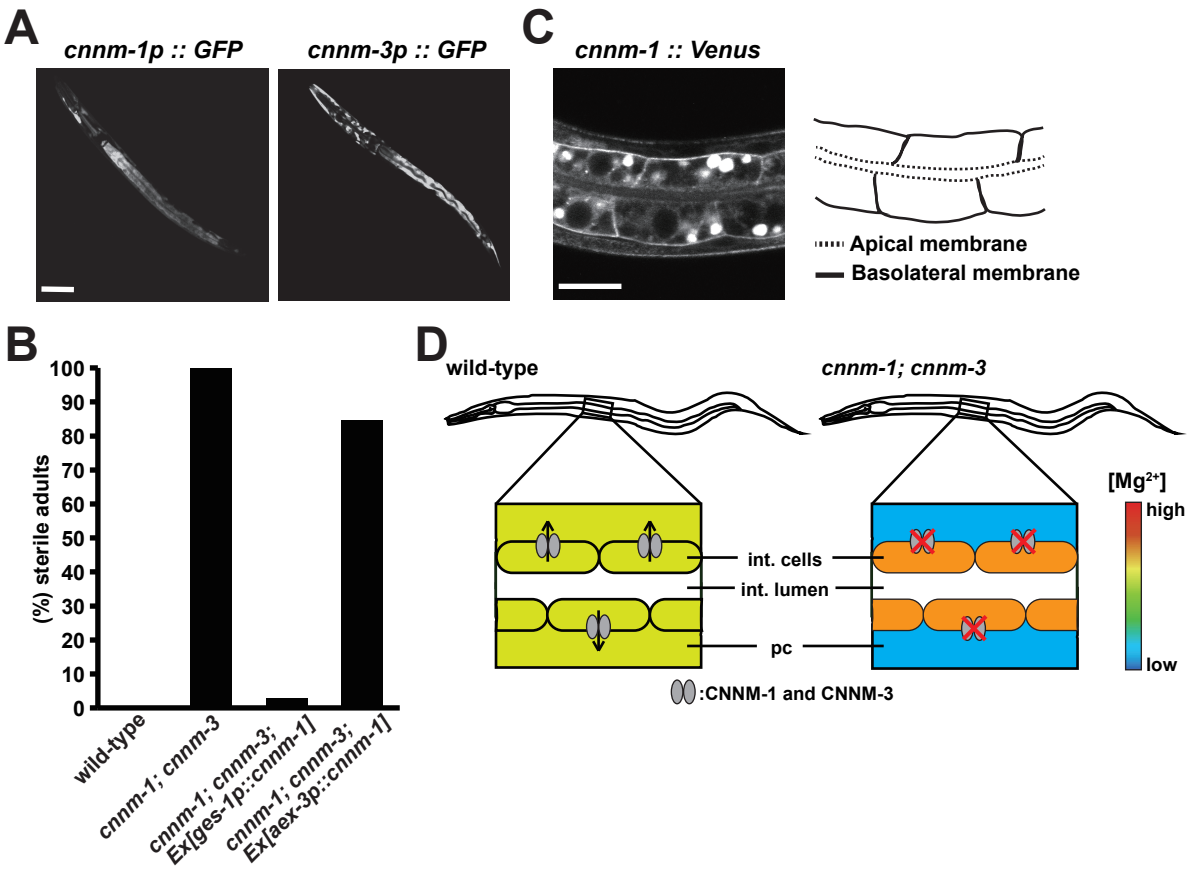
A
cnnm-1p :: GFP
cnnm-3p :: GFP
C
cnnm-1 :: Venus
Apical membrane
Basolateral membrane
B
(%) sterile adults
100
90
80
70
60
50
40
30
20
10
0
wild-type
cnnm-1; cnnm-3
cnnm-1; cnnm-3; Ex[ges-1p::cnnm-1]
cnnm-1; cnnm-3; Ex[aex-3p::cnnm-1]
D
wild-type
cnnm-1; cnnm-3
int. cells
int. lumen
pc
:CNNM-1 and CNNM-3
[Mg2+]
high
low

Figure 11

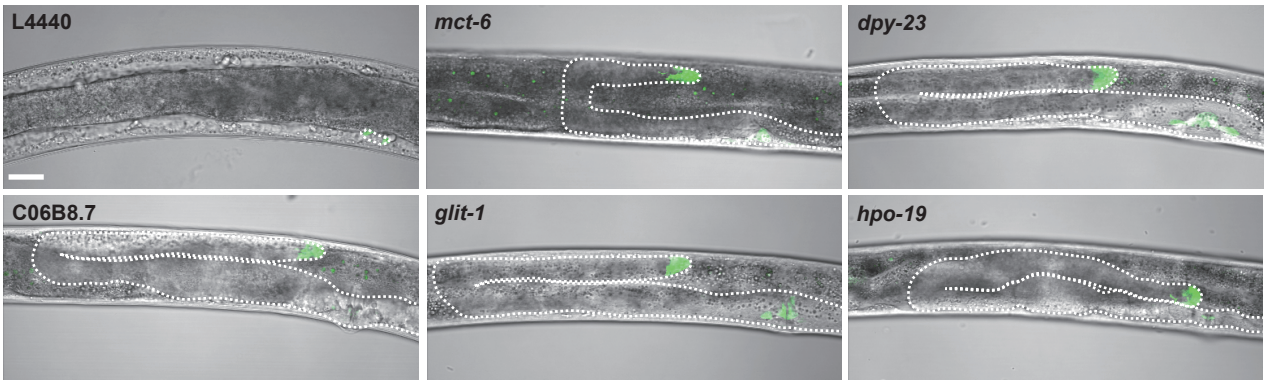

Figure 12

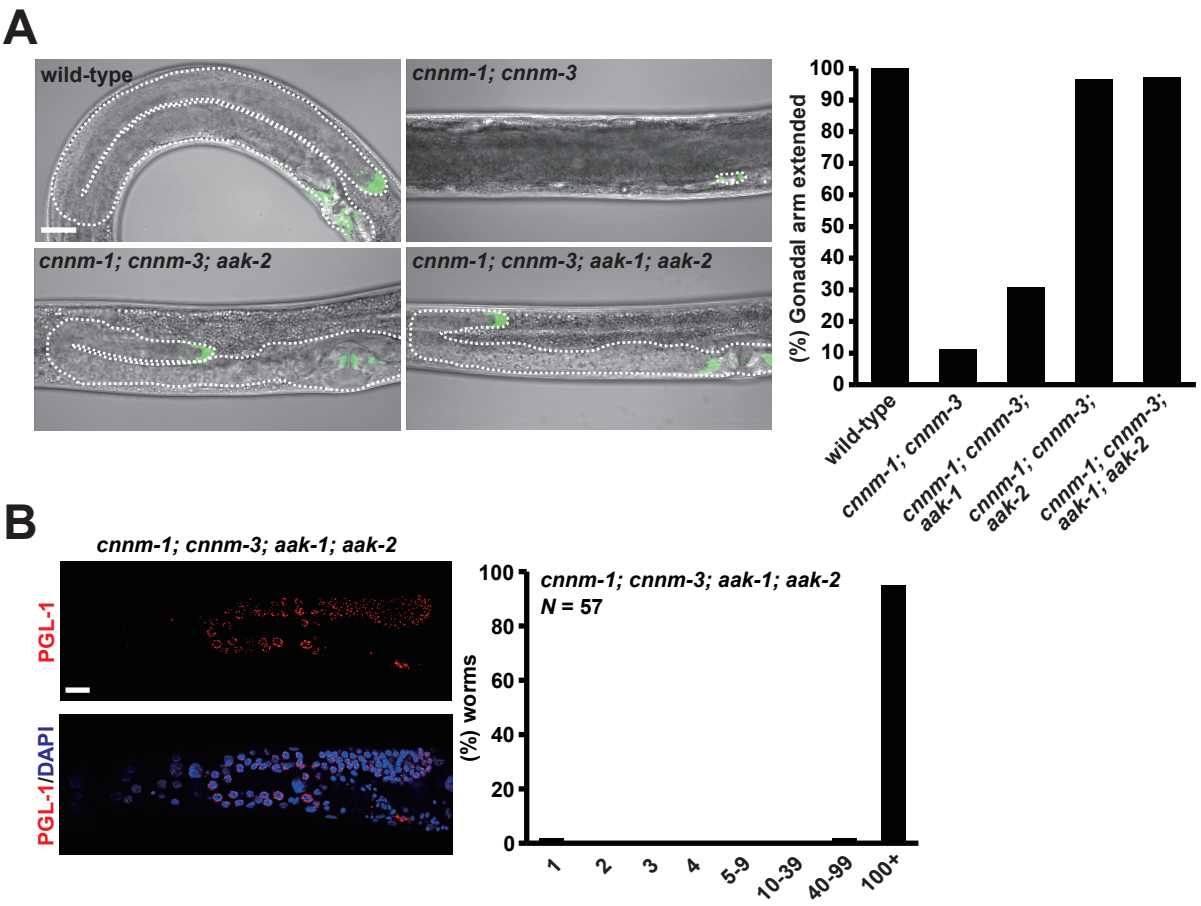
A
wild-type
cnnm-1; cnnm-3
cnnm-1; cnnm-3; aak-2
cnnm-1; cnnm-3; aak-1; aak-2
(%) Gonadal arm extended
100
90
80
70
60
50
40
30
20
10
0
wild-type
cnnm-1; cnnm-3
cnnm-1; cnnm-3; aak-1
cnnm-1; cnnm-3; aak-2
cnnm-1; cnnm-3; aak-1; aak-2
B
cnnm-1; cnnm-3; aak-1; aak-2
PGL-1
PGL-1/DAPI
cnnm-1; cnnm-3; aak-1; aak-2
N = 57
(%) worms
100
80
60
40
20
0
1
2
3
4
5-9
10-39
40-99
100+

Achievements

Publication

1. **Ishii T**, Funato Y, Hashizume O, Yamazaki D, Hirata Y, Nishiwaki K, Kono N, Arai H, and Miki H. Mg^{2+} Extrusion from Intestinal Epithelia by CNNM Proteins Is Essential for Gonadogenesis via AMPK-TORC1 Signaling in Caenorhabditis elegans. **PLoS Genet.** *12*, e1006276 (2016)

2. **Ishii T**, Funato Y, and Miki H. Thioredoxin-related Protein 32 (TRP32) Specifically Reduces Oxidized Phosphatase of Regenerating Liver (PRL). **J. Biol. Chem.** *288*, 7263-7270 (2013)

Presentation

1. Mg^{2+}トランスポーターCNNMはAMPKを介して線虫の生殖巣形成を制御する

   第88回日本生化学会大会、神戸、2015年12月　（口頭発表）

   石井匡、船戸洋佑、平田祐介、三木裕明

2. TRP32はがん転移因子PRLを特異的に還元する

   第85回日本生化学会大会、福岡、2012年12月　（ポスター発表）

   石井匡、船戸洋佑、三木裕明

Research fellowship

1. Research Fellowships for Young Scientists (DC2)

   Japan Society for the Promotion of Science, April 2014 – March 2016.